

Automatic Breast Cancer Cell Classification using deep Convolutional neural Networks

Authors: Gisela Pattarone
Submitted: 30. March 2020
Published: 3. April 2020
Volume: 7
Issue: 2
Affiliation: Faculty of Pharmacy and Biochemistry, Faculty of Medicine – Universidad de Buenos Aires, Argentina and Faculty of Medicine – Albert Ludwigs University of Freiburg, Germany
Languages: English
Keywords: breast cancer cell, medicine Program, Argentina, Germany, biomedical Sciences
Categories: Medicine, Artificial Intelligence, Modeling and Simulation
DOI: 10.17160/josha.7.2.652

Abstract:

Automated cell classification in cancer biology is an active and challenging task for computer vision and machine learning algorithms. In this Thesis, we first compiled a vast data set composed of JIMT-1 human breast cancer cell line images, with and without therapeutic drug treatment. We then train a Convolutional Neural Network architecture to perform classification using per-cell labels obtained from fluorescence microscopy images associated with each brightfield image. The study revealed that our classification model achieves 65% accuracy in breast cancer cells under chemotherapeutic drug treatment with doxorubicin and paclitaxel. Furthermore, it reached 70% accuracy when classifying breast cancer cells without drug treatment. Our results highlight the potential of machine learning and image analysis algorithms to build new diagnosis tools.

JOSHA

josha.org

**Journal of Science,
Humanities and Arts**

JOSHA is a service that helps scholars, researchers, and students discover, use, and build upon a wide range of content



Automatic breast cancer cell classification using deep convolutional neural networks

For the degree of Master of Science

Author: MD. Gisela Pattarone

Cohort: 2018 - 2020

Director: Prof. Dr. Joschka BÖDECKER

Co- Director: Dr. Emmanuel IARUSSI

Faculty of Pharmacy and Biochemistry, Faculty of Medicine –
Universidad de Buenos Aires, Argentina

Faculty of Medicine –
Albert Ludwigs University of Freiburg, Germany

[2019]



UBA
1821 Universidad
de Buenos Aires



IMBS
International Master Program
in Biomedical Sciences



Author: Gisela Romina PATTARONE

Director: Prof. Dr. Joschka BÖDECKER

Co- Director: Dr. Emmanuel IARUSSI



UBA
1821 Universidad
de Buenos Aires



IMBS
International Master Program
in Biomedical Sciences



Master of Science in Biomedical Sciences

Statement for the Master's Thesis

Hereby I confirm that

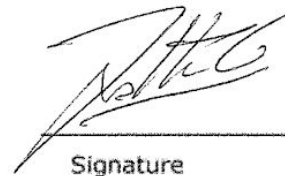
- I completed the submitted master's thesis independently.
- I used no sources or aids other than those stated and all verbatim or conceptual content taken from other works has been identified as such.
- the submitted master's thesis was or is not, either in full or in large part the subject of another examination process.
- the electronic version of the master's thesis submitted is in content and format the same as the printed version, and
- the master's thesis has not yet been published.

November 20th 2019

Date

GISELA PATRONE

Name, Firstname



Signature

1. Abstract

Automated cell classification in cancer biology is an active and challenging task for computer vision and machine learning algorithms. Breast cancer is the most common malignancy in women and involve phenotypically diverse populations of breast cancer cells tumoral heterogeneity. The heterogeneity of the cells within the tumors can influence their biological behavior and the therapeutic response. Over the last few years, there have been several studies orientated to build an artificial intelligence-based cell classifiers using label-free brightfield cell images. However, to our knowledge there is no previous work attempting to perform individual cellular segmentation and classification for breast cancer using imaging techniques. In this Thesis we are interested in classifying breast cancer cells based on their morphological characteristics using automatic image processing techniques, without any staining and using only brightfield images as input. To this end, we first compiled a vast data set composed by JIMT-1 human breast cancer cell line images, characteristically resistant to chemotherapy, with and without therapeutic drug treatment. We carefully describe the acquisition conditions and setup in sections 5.5. We then train a Convolutional Neural Network (section 5.6) architecture to perform classification using per-cell labels obtained from fluorescence microscopy images associated to each brightfield image. Our CNN was evaluated on a large number of brightfield images of JIMT-1 cells. The study revealed that our classification model achieves 65% accuracy in breast cancer cells under chemotherapeutic drug treatment with doxorubicin and paclitaxel. Furthermore, it reached 70% accuracy when classifying breast cancer cells without drug treatment. Our results highlight the potential of machine learning and image analysis algorithms to build new diagnosis tools that benefit the biomedical field by reducing cost, time, and stimulating work reproducibility.

2. Acknowledgements

The work of this Thesis is divided between the two countries: Germany and Argentina. I greatly appreciate the efforts of both universities to achieve a master's degree with a binational program. Thank you very much to the directors of both universities and the program, as well as to the administrative ones that support all our organization.

Regarding the work of this Thesis in Germany, I want to thank the opportunity to met Professor Roland Mertelsmann. Who with his innovative ideas made me believe that this work was possible to carry out and supported me completely in each of the adversities that arose along the way. In addition, I want to thank the entire research team in Germany: my director Joschka Bödecker, supervisor Marie Follo, and my lab partners and friends Dario Ruarte, Ana Peñaherrera and Gustavo Rosero. They somehow constituted to shape not only this project but also me as a researcher with their explanations, effort, support, discussion and co-learning experience. Also thank the Core Facility that allowed us to develop our experiments day and night in their halls and rooms.

Regarding the work of this Thesis in Argentina, I want to thank completely to my co-director Emmanuel Iarussi. Who, without knowing me and having contacted him by a simple e-mail believed in me and in the project from the moment zero. As well as he dedicate hours, tools and multiple talks, videos, courses to teach me each of the bases and techniques of the new tools I was learning about programming and machine learning.

On the other hand, as happens in a Thesis and in life, almost nobody is made just with their own thing. Likewise my training as a researcher happened day by day, so did my life and each one of the experiences. For this reason, I want to dedicate a very special section for my family and friends, who accompanied me and supported my dream, they saw me work it, stumbling and getting up again and again, to finally finish and conclude it, always walked and stayed by my side.

Simply, thanks.

3. Abbreviations and Symbols

Live/dead kit fluorescence: calcein and propidium iodide (LC).

Apoptosis activity by caspases 3 and 7 fluorescence (AP).

Autophagy activity fluorescence (AG).

Propidium iodide fluorescence: caspase-independent cell death process (PI).

Lab on a Chip (LOC).

Low-dose metronomic (LDM) chemotherapy.

Human Epidermal growth factor Receptor 2 (HER2).

Basal cell-like (BCL) breast tumor.

Immunohistochemical (IHC).

Estrogen receptor (ER).

Progesterone receptor (PR).

Epidermal Growth Factor Receptor(EGFR).

Reactive Oxygen Species (ROS).

Caspase-independent cell death (CICD).

Cancer-associated fibroblasts (CAF).

Breast Cancer Cells (BCC).

Convolutional Neural Network (CNN).

FIJI (Fiji Is Just ImageJ).

Polidimethylsiloxane (PDMS).

Phosphate buffer solution (PBS).

Region of interest (ROI).

Open Source Computer Vision Library (OpenCV).

Graphics Processing Unit (GPU).

Doxorubicin(DOX).

Paclitaxel(PAX).

Stochastic gradient descent (SGD).

True Positive (TP).

False Negative (FN).

True Negatives (TN).

False Positive (FP).

Area Under The Curve - Receiver Operating Characteristics (AUCROC).

True Positive Rate(TPR).

False Positive Rate (FPR).

4. Content

1.- Introduction

Cancer biology research has been taking part over the last four decades (Hanahan, D., 2011), inspired by relieving and destroying malignant growth. Breast cancer is the most common malignancy in women (Arabsalmani, M., 2017). Cancer is not a single disease and involves biologically diverse populations, with not only different pathological characteristics and clinical implications, but also with high intratumor heterogeneity. There is an important intricacy of molecular cross talk within the cell death pathway that highlights the need for developing more *in vitro* studies to characterize the morphological response to the different anticancer drugs. In this Thesis, we first propose to characterize the biological behavior of breast cancer cells (JIMT-1) with different stainings to evaluate: cell viability (LC), apoptosis activity by caspases 3 and 7 (AP), autophagy activity (AG), caspase-independent cell death process (PI), inside of Lab on a Chip (LOC) devices. We study cellular growth before and after the introduction of two different types of schematic drugs treatments applied *in vivo* to breast cancer cells. On the one hand, Paclitaxel demonstrated initial activity in breast cancer and combined with doxorubicin constitutes the most active known agent for breast carcinoma with different schedules. In the other hand, low-dose metronomic (LDM) chemotherapy is a novel form of chemotherapy utilization, defined as conventional at low doses with no prolonged drug-free breaks. This study of biological behaviour was addressed with high microscope technology that allows live cell imaging over extended time periods, while simultaneously associating brightfields with their fluorescence microscopy counterparts. By cultivating and performing high-resolution microscopy of JIMT-1 cancer cell line, we have developed a vast data set of images. we hypothesize that we can gain a deeper knowledge from this massive biomedical *in vitro* data set by means of machine learning and image processing techniques. These algorithms simplify the process of processing large amounts of images, automatically extracting the underlying patterns in the data. In this Thesis we automatically classify cancer cells without any staining and using only brightfield images as input at testing time. We believe his approach could be

used as a diagnostic and complementary tool for cancer and normal cell biology, allowing a greater understanding of the capabilities of image-based automatic classification. Furthermore, these tools have potential applications in the pharmaceutical field, as automatic dead cell classification in clinical trials for drug tests must be of high interest, complementing the information related to pharmacokinetics and pharmacodynamics characteristics in vivo from an anti-cancer drug.

1.1- Breast Cancer subtypes

The breast cancer biological diversity is reflected in the magnitude of analyses performed in this field. Initially, pathologists standardized the taxonomy based on their morphological characteristics. Then, with the development of microarrays, the gene expression profiling took a more important place for being used in breast cancer prognosis. One of the most important studies use 456 cDNA clones and develop a molecular portrait of breast cancer (Perou, C., 2000). This study reports at least five main subtypes of breast cancer tumors: luminal A, luminal B, Erb-B2 tumors with the Human Epidermal growth factor Receptor 2 (HER2) over-expression, basal cell-like (BCL) and normal breast-like group (Table 1). This classification has been used specially for breast cancer prognosis. The new paradigm of gene classification showed that the cancer cell response to treatment is not defined by anatomical and histological grades. The microarrays classification were included with the classical immunohistochemical (IHC) markers associated with breast cancer cells: estrogen receptor (ER), progesterone receptor (PR) and HER2. Fundamental differences at the molecular level of the tumors have implications in the management of therapeutic decisions. Finally, several studies have shown that the relationship between IHC markers and stratification of breast cancer it is important for the response to therapeutic treatments. According to this IHC markers, the final classification involve luminal A and B are ER positive, BCL have a phenotype known as “triple negative” because they are ER, PR negative and the gene Her2/neu is also negative.

Intrinsic subtype	IHC status
Luminal A	[ER+ PR+] HER2-KI67-
Luminal B	[ER+ PR+] HER2-KI67+
Luminal B	[ER+ PR+] HER2+KI67+
HER2 over-expression	[ER-PR-] HER2+
Basal	[ER-PR-] HER2-, basal marker+
Normal-like	[ER+ PR+] HER2-KI67-

Table 1 - Summary of the breast tumor molecular subtypes

Good prognosis and less aggressive behaviour are associated with the presence of the receptors in Luminal subtypes compared with the BCL or Her2/neu groups which has been usually associated with lack of response to the usual therapies and poor clinical outcomes (Spitale, A., 2009). HER2 is a receptor tyrosine kinase present in the membrane of the cells (Figure 1). The extracellular half is designed to recognize ligand-activated forms of it family members like Epidermal Growth Factor Receptor(EGFR) leading to dimerization. After this event, the cytoplasmic part of HER2 contains a catalytic kinase domain that finish with the phosphorylation of tyrosine cytoplasmic residues and the recruitment of second messenger proteins to these phospho tyrosines. In breast cancer cells, when the gene is amplified, the result is a massive overexpression of HER2 with the consequent activation of numerous downstream ligand-stimulation mechanism with the correlate activation of different biological pathways that promote the malignant phenotype (Saenz, A., 2018).

HER-2-oncogene targeting drugs development concentrates a big part of the effort in this field. This context guided to the development of trastuzumab (Herceptin), a humanized monoclonal HER2 antibody with a remarkable clinical response of 40% when is used as a single agent for first-line treatment against HER2-overexpression metastatic breast cancer. Despite this, clinical resistance exists and its study is obstructed by the narrow circumstances of suitable

experimental model systems.

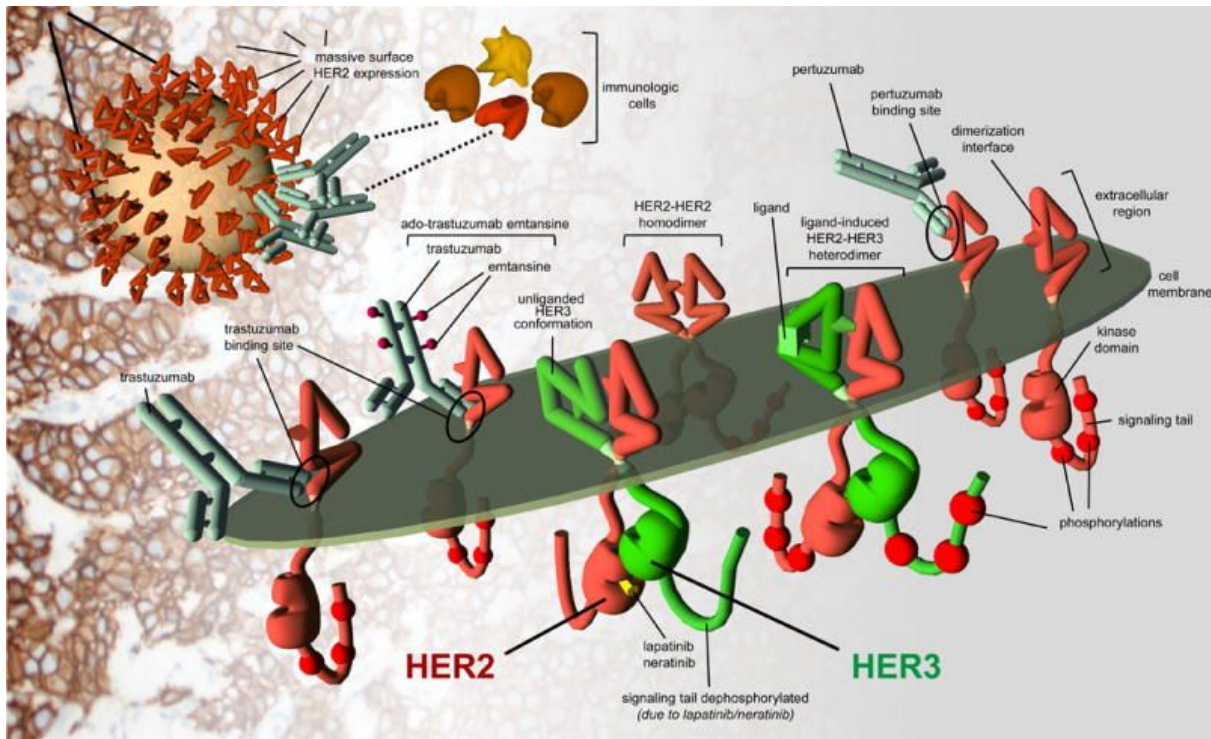


Figure 1- Schematic shows the expression of HER2 on the surface of HER2-amplified cancer cells as seen on HER2 immunohistochemistry (background image) and as imagined by schematic drawings.¹

This context guided researchers to establish a new carcinoma cell line, namely JIMT-1 (Tanner, M., 2004). The new line was obtained from a pleural metastasis of a 62-year old patient with breast cancer who was clinically resistant to trastuzumab. Characteristically, JIMT-1 cells grow as an adherent monolayer and have an amplified HER2 oncogene without identifiable mutations on its coding sequence. Furthermore, the cell line lacks expression of estrogen and progesterone receptors. These implies that they act like a triple negative subtype. Phenotypically has analogies with epithelial cells evidenced by

¹ Extracted: Saenz, A, Targeting HER2 by combination therapies. J Clinical Oncology, 2018; 10, 808-811

immunohistochemical positivity for cytokeratins 5/14 and 8/18.

1.2- Breast Cancer chemotherapy

The management of the therapeutic decision in breast cancer also include chemotherapy and hormone therapy in different combinations. Paclitaxel has been one of the most used drugs against breast cancer (Reichman, B., 1993). It was discovered in 1962 as a result of a screening program developed by the Cancer Chemotherapy National Service Center of the United States. Later, it was isolated from the bark of the Pacific yew, *Taxus brevifolia*, from which is derived its name: "taxol". Its an antineoplastic agent known as the taxanes family that demonstrate a novel mechanism of action characterized by the promotion of the assembly of microtubules and their stabilization. This acts against depolymerization and results in mitotic arrest cellular state (Long, H., 1994). Doxorubicin, another chemotherapy agent, has been used like an adjuvant in different BCC (Karuppaiyl, S., 2018). It is an anthracycline drug extracted from *Streptomyces peuceti* discovered in 1950 as a result of the effort from an Italian research company to find anticancer compounds from soil-based microbe. Doxorubicin is a transcription inhibitor acting through inhibition of DNA-dependent RNA polymerase and is a DNA intercalator leading to DNA strand breaks and formation of Reactive Oxygen Species (ROS) in cells. Literature support different chemotherapeutic strategies with different schedules and combination against breast cancer cell lines. In triple negative cases there are two different promising strategies. Nowadays paclitaxel is combined with doxorubicin, a sequential treatment with 4 hr of doxorubicin followed by 24 hr of paclitaxel has shown synergistic cytotoxic effect validated in clinical phase I/II study of patients with advanced stages of breast cancer (Amadori, D., 1996). On the other hand, low-dose metronomic (LDM) chemotherapy is a novel and alternative chemotherapy approach for resistant cases. This therapy is defined as the administration of low doses of paclitaxel on a regular and frequent daily schedule, with no prolonged drug-free periods (Lien, K., 2013).

1.3- Tumor heterogeneity Biology

The different subtypes of breast cancer imply a complexity that is enhanced by tumor heterogeneity. In the literature this aspect is usually divided into inter-tumoral and intra-tumoral heterogeneity. Basically, inter-tumoral heterogeneity is defined as genotypic and phenotypic variations founded between a primary tumor and a metastatic lesion of the same type from one patient. While intra-tumoral heterogeneity is referred to biological variations that happen within a single patient risen by the coexistence of different cell population with a crucial role in tumor expansion and therapeutic resistance. Observations made in several individuals (Turashvili, G., 2017) show mechanism activity of intra-tumoral heterogeneity related to the tumor microenvironment. This biological behaviour affect the rate of tumor development, which involve at least proliferation and apoptosis unregulated, and the therapeutic response to chemotherapeutic agents. Accumulative evidence suggested that common anticancer drugs strategies have to consider the different behaviour exhibited because they were playing their roles within different cell death modes discovered related to tumorigenesis microenvironment, including caspase-dependent apoptosis, caspase-independent cell death, reproductive cell death (cell senescence), or cell death dependent on autophagy (Leist, M., 2001).

1.4- Cell death modes in Cancer Biology

Remarkable advances in cancer biology and cancer genetics have shown that apoptosis and the genes that control it have a malignant phenotype. There is evidence that some oncogenic mutations promote tumor initiation disrupting apoptosis and have consequences on growth and progression. On the other hand, compelling evidence indicates that another mutations could promote apoptosis, producing a selective pressure to disallow it during different carcinogenesis stages. Associated to this scenario, most cytotoxic anticancer agents induce apoptosis, raising the engaging evidence of the fact that apoptotic programs contribute to treatment failure (Lowe, S., 2000). Moreover, apoptosis initiated by mitochondrial outer membrane permeabilization usually leads to caspase activity

in cells that could promote genomic instability, potentially boosting tumour evolution. The same mutations that suppress apoptosis during tumor development also reduce treatment sensitivity. This situation makes it necessary to find a better diagnostic approach. A different direction is taken by the process called caspase-independent cell death (CICD). According to literature, to promote the inhibition of caspase downstream of the mitochondrial outer membrane permeabilization can trigger necroptosis as a cell death mode. This produces several amount of different cytokines, like pro-inflammatory TNF which finally promote an autocrine necroptosis effect (Giampazolias, E., 2018). Another important focus of the tumor microenvironment is the relationship between the role of cancer-associated fibroblast (CAF) and senescent cells, since both can change their tissue microenvironment. CAF can develop a pro-tumorigenic state and senescent cells could act with a dual role. On the one hand, senescent cells act like a role of cancer protection because they lose the ability to undergo in a permanent cell division activity, although they may be metabolically fully active. This would protect the final state of a primary cancer in a cancerous growth. On the other hand, the role of cancer promotion is strongly represented by different hallmarks of cancer. Senescent cells may have genetic and epigenetic instability and, in the secretory phenotype, they could destroy the extracellular matrix which helps to spread cancer cells in the body. In this backdrop one of the anticancer drug strategies in terms of cytostasis could be an alternative way in which cellular senescence offers a promising strategy to stop proliferation of cancerous cells (Schosserer, M., 2017). Although results from different studies tend to be consistent about cellular senescence acting as a critical anticancer mechanism, there is still no evidence of anticancer drug effects related to senescence activity. Another CICD is named in the literature as autophagic type II cell death, being apoptosis-caspase dependent the type I. From reviewing the field literature, it becomes evident that autophagy and apoptosis seem to be interconnected positively or negatively and mitochondria is the organelle that integrate them. Implication of tumor suppressors like Beclin 1, DAP-kinase and PTEN in autophagic pathways indicate an association between malignant transformation and suppression of autophagy. Autophagic vesicles are typically characterized by

the appearance of double membranes where their content are usually destroyed by the lysosomal system. Their overall activity is more extensive when a cell is doomed to die. It has been well documented a correlation between reduced autophagy and cancer, it means that a failure in autophagy signaling could be fundamental in cancer formation, working as a mechanism that restricts uncontrolled cell growth (Gozuacik, D., 2004). Some cancer cell types respond to anticancer drugs by triggering autophagy. This reflects the priority of considering their induction as a new cancer treatment modality and the need to understand better the correlation with the current therapies and their possible effects. Concerning the literature, in only one strict type of cell death 1 or 2 it is suggested that a lethal process could be marked initially with autophagic vacuolization of type 2 cell death. Then, shift to a process marked by the final mitochondrion-dependent caspase activation with nuclear apoptosis.

1.5- In Vitro strategies for intratumor heterogeneity studies

It is clear after this exposition that most effort should be oriented to assess intratumor heterogeneity in order to develop more effective treatments with less adverse effects. Also, these intricacy of molecular cross talk within the cell death pathway highlights the importance of more in vitro studies that characterize the morphological response, not only to cell growth, but also to different anticancer drugs. According to this, one in vitro strategy developed for single cell analysis was the miniaturization of basic conventional biological or chemical laboratory operation, like microfluidic models. The development of micro devices is an interesting alternative since they offer a large surface/volume ratio, and a more homogeneous and controllable microenvironment. Within the microfluidics devices, some laboratory operations are developed. These operations are related to sample injection and reagents in order to promote growthment and isolation of cells (Xu, Z. 2014, Leckler E., 2003). These microsystems are identified as Lab On a Chip (LOC) (Cheong, R. 2009). Their characteristics make them especially suitable for cancer cytology research, considering that tumor cells presented an improved response to viability, invasion and variable drug response, when seeded in LOC culture systems (Liu et al., 2009, 2010). More interesting is the fact that

studies based on microfluidics opened the way for integrated cytological, genomic, and proteomic analysis that identified hundreds of new biomarkers potentially involved in tumorigenesis. Certain LOC devices are designed for cytological analysis and allow analysis at the single cell level (Zare, R. 2010). Allowing the monitoring of a cell by studying its growth characteristics and biological behavior represent a powerful tool to detect intracellular changes for live cell imaging. Furthermore, these devices are especially suitable for live-cell fluorescence staining of the different cell death modes promoted by the therapeutic schemes and for tracking it with automatic microscope technologies.

1.6- Image analysis with Machine Learning techniques

The emergence of automatic microscopes made it possible to develop large data sets for biomedical science, but pre-processing and organizing data to be useful requires a thorough analysis. For centuries, scientists have trained themselves to look and detect structural and molecular features. However, this changed with the emergence of digital data, correlated with the development of Computer Science that allowed to extract information from massive biomedical data sets. More data comes with the need for new algorithms, techniques, and analytics to explore and interpret them in their specific scale, diversity and complexity. Usually biomedical data is entirely characterized as the 4Vs: volume, velocity, variety and veracity (Choong, H., 2017). Literature in the field summarizes different areas of application of big data. In this Thesis we are particularly interested in applications to improve healthcare. For example, the work of Raul C. Deo (Deo RC., 2015), it is particularly useful to understand the implications of different applications of machine learning in Medicine. Among them, we can mention population management, and development of predictive disease models with learning from data. The goal of big data analysis is finding human-interpretable patterns and associations, using automatic extraction of unknown information from large data sets using advanced computational techniques and algorithms. However, these algorithms usually require lots of data. Therefore, creating large biomedical data sets it is of paramount importance to develop new diagnosis tools that profit from

Machine Learning techniques.

Algorithms in data mining are categorized as unsupervised, semi-supervised and supervised learning. The last category works by means of a training set which is augmented with pre-classified data in order to learn a model capable of predicting this known labels. Unsupervised learning groups algorithms that analyze data in order to find naturally occurring patterns without a labeled input to predict. Between both we have semi-supervised learning algorithms that use small data sets of labeled and much larger unlabeled data collection to balance performance and precision of the output (Maetschke, S., 2014). In this work we tackle a supervised learning classification problem.

1.7- Convolutional Neural Networks for cell classification

Analytic aims of medical big data are prediction, modeling and inference. The methods in these context are classification, clustering and regression. Classification, generally a supervised problem, it is used for predictive modeling where the output is categorical in terms of a vector or predicting variable. Classification involves rule construction in order to assign objects to one of the predicting variables or the pre-specified set of classes. This assignment is based on a measurable vector taken on the input objects to be classified. One very popular classification method is called *Neural Network* (NN). For example, NNs can be used to build a model able to predict a prognosis based on data labeled with biomarkers, or develop a decision support system able to design a specific label among several possible labels. Another task we can perform with this family of algorithms is clustering (Glassner, A., 2018). Generally, unsupervised learning it is used to find aggregates in the data using distance metrics, with the following supervised evaluation of the performance. Clustering can be found in microarray data analysis and it is also used to better approach the pathophysiologic mechanisms, providing therapeutic options. Before applying any of these methods, a preprocessing step it is crucial to have satisfactory results. Preprocessing consists in data set selection, cleaning, and reduction of variables for efficiency. Then, Machine learning algorithms can processes and learn from

these data, automatically deducing the underlying patterns in them. In recent years, the state of the art in automatic classification of images has become dominated by Deep Learning techniques (LeCun, Y., 2015), a form of automatic learning (Asri H., 2016). Label-free cell classification could offer substantial improvements in detection specificity, sensitivity and accuracy for physiological and pathological cell condition diagnosis. In the context of this Master Thesis, visually inspecting the cellular structure for biological samples can be a very challenging task. Apart from the high variability of the samples, visually analyzing the cells structure it is hard due to the poor refractile characteristics and the amplification of the contrast by optical and electronic techniques when using fluorescence labeling with dyes that have the goal of reveal macromolecular structures. Since fluorescence labeling has limitations, we decided to exploit a deep learning approach to automatically perform image classification. Close to our work is Christiansen, E., 2018, who designed a deep neural network and trained it with labeled images from different cell types like motor neurons, stem cells, and breast cancer cell line. In order to obtain labels for each cell, they proposed to use Hoechst or DAPI to label cell nuclei, CellMask to label plasma membrane and Propidium Iodide to label cells with compromised membrane. They tested their automatic labeling network using unlabeled testing images and were able to make accurate pixel predictions of the location and intensity of the different structures represented by the fluorescence. Furthermore, they presented a proper method for live cells prediction with no additional sample preparation and minimal impact on the performance. These techniques are improving quickly with the emergence of new algorithms and innovative biological applications, such as the morphological classification of hematopoietic cells, pluripotent stem cells (Kusumoto D., 2018) and mycobacteria in macrophages (Xinzhuo, Z., 2019). Empowered by the new machine learning image processing architectures, in this Thesis we present a massive data set of breast cancer cell images of JIMT-1 type. Each cell has been individualized and properly tagged in one of these four categories: cell viability with calcein and propidium iodide, autophagy process and caspase activity. Also, we collect nuclear information with H \ddot{o} echst staining. To our knowledge, this is the biggest data set of its type ever compiled. We then show

how this data can be used to train a Neural Network for cell image classification. Our trained classifiers can label cancer cells as live or dead without any staining and using only brightfield images as input.

2.- Objective, Hypothesis and Aims

The goal of this Thesis is twofold. First, since training deep learning algorithms requires a large amount of organized labeled data, we aim for the creation of a large data set of cancer cell images using microfluidic systems like Lab On a Chip (LOC). These systems allow the analysis of cell growth characteristics during all the phases of the growth and treatment of adherent cells (Breast Cancer Cells (BCC)) in real time. We plan to capture cancer cell images in four different scenarios and label their biological process (cell viability: live and dead, autophagy and apoptosis) using fluorescence live cell imaging. Second, we train an automatic classifier using our custom data set which is able to label live/dead cell states from the morphological characteristics of the microscopy cell images (brightfield).

We propose to break down the aforementioned general objectives into the following specific goals:

SO1. Generate a database of representative images of the biological behaviour of BCC with different staining to evaluate cell viability, apoptosis programmed and autophagy.

SO2. Complement the database with images of BCC treated with anti-cancer drugs cultured in LOC devices.

SO3. Segment individual cells in brightfield images and label them with the correspondent biological state according to the staining information recovered from the microscope.

SO4. Define and train a Convolutional Neural Network (CNN) able to perform automatic cancer cell image classification without requiring fluorescence staining.

SO5. Evaluate the accuracy of the learned models with images under different capture conditions. We also plan to evaluate the generalization power of our network to classify other BCC lines with different biological characteristics such as triple positive receptors.

SO6. Compare the results of traditional methods like FIJI (Fiji Is Just ImageJ) used for train a classifier and segment data of growth rate according to administration of treatment and area covered by cells in microdevices.

3.- Research Plan

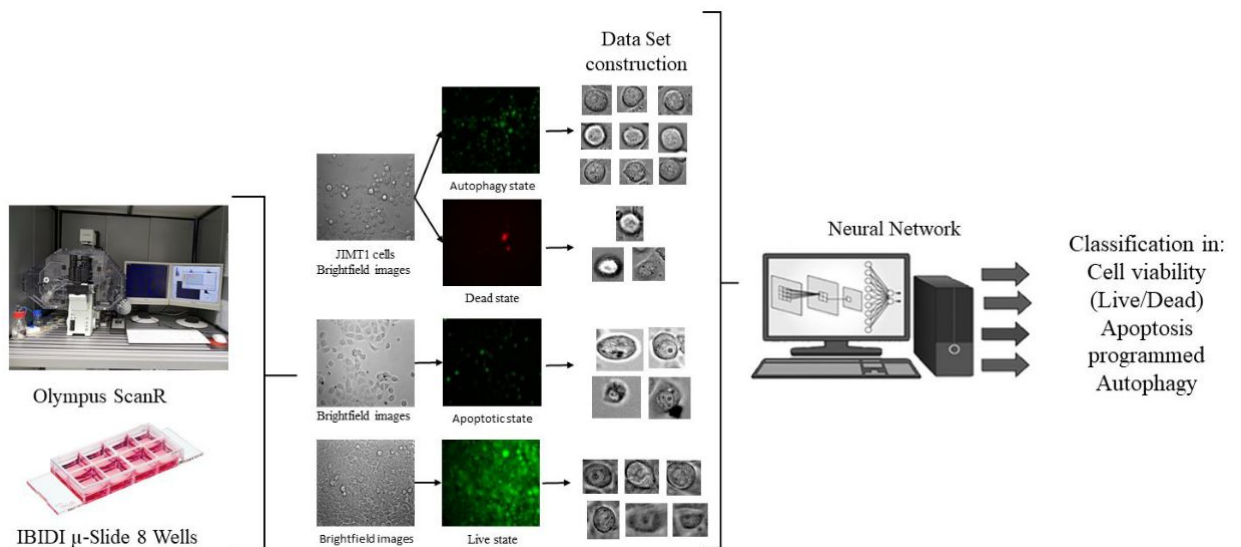


Figure 2 - General pipeline of our approach. First, images are collected using Olympus ScanR microscope. We then automatically segment and label each cell using image processing techniques. Notice that automatic segmentation and labeling may not extract the same number of images on each input sample. Finally, we train a Convolutional Neural Network that can automatically classify new unseen cells.

As shown in Figure 2, we first use Lab On a Chip (LOC) devices to study and characterize the biological behaviour of breast cancer cells (JIMT-1) with different staining to evaluate: cell viability(live/death), apoptosis programmed (caspases apoptosis), spontaneous resistance(autophagy), apoptosis (death process), inside μ -Slide 8 wells- (Ibidi GmbH) devices before and after to introduce two different types of schematic drugs treatment applied in patients with breast cancer cells. Furthermore, images of each characteristic were acquired by ScanR microscope.

Second, the compiled images undergo a curation process to individualize cells (detect and segment them). In addition to the segmentation, each individual cell needs to be tagged with a label indicating the classification category it belongs to, obtained from the associated staining image. We gather more than 40000 images in total. In particular, we are inspired by the work of Xinzhuo Zhao who develop a semi-supervised learning method to detect and extract infected and uninfected cells (Gonzalez, R., 2008). Even if working with different cell types, the same curation process is common to most image processing and computer vision applications . The curated data set it used to learn the parameters of a Convolutional Neural Network (Goodfellow, I., 2016) able to perform automatic classification of cell's death modes. In a later stage, the learned model could be useful to perform recognition of the biological behaviour regardless of staining images.

4.- Materials and Methods

The following is a description of the specific methodologies and experiments carried out, the proposed objectives, and validate the working hypothesis.

Regarding specific objectives 1, 2, and 6:

4.1.- Microfluidic devices: design and manufacturing.

The microfluidic devices consist of an input and an output connected to four micro-channels of 500 μ m width with eleven circular chambers (1250 μ m of radius)

connected within each micro-channel, having a total internal volume of 150 μl . The layouts were designed using Klayout editor software (<http://www.klayouteditor.de>). Photopolymer flexographic master mold (Fmold) and epoxy resin mold (ERmold): The microdevices were fabricated in polydimethylsiloxane (PDMS). For this purpose, a master mold of the design was fabricated in high relief with printing plate photopolymer Flexcel SRH and DITR film as previously described by Olmos et al. Briefly, the design was transferred to the DITR film with an infrared laser source of 2400 ppi. Then, the film was laminated onto the unexposed flexographic printing plate before being exposed to UVA light at 0.45 J on the reverse side and UVA light at 19 J on the front for 360s. After the exposure, the film was removed. Then, the flexographic printing plate was washed with solvent PROSOL N-1 at 360 mm min⁻¹ and dried in an oven during 30 min at 50 °C. Finally, flexographic printing plate was exposed to UVC light at 10 J for 17 min and UVA light at 4 J for 2 min on the front. This mold was called Fmold. The Fmold before to used was placed in an oven at 100 °C for 12 hr and then it was treated in a vacuum chamber for 1 hr at 25 °C. Afterwards, the cleaning process was performed in 70% ethanol solution in an ultrasonic bath for 7 min, dried at 40 °C for 10 min and cleaned by a nitrogen stream. Then epoxy resin and curing agent (Cristal-Tack, Novarchem - Argentina) were mixed by hand-stirring for 3 min in a 2:1 weight ratio and ultrasonically treated using a bath-type sonicator (TESTLAB Ultrasonic Cleaner) for 7 min to remove air bubbles. Then, the mixture was poured onto the Fmold and cured at room temperature for 72 hr. After curing, the epoxy resin mold was peeled off from the Fmold to form the male mold and called as ERmold²⁹.

PDMS microdevice: Briefly, the PDMS was mixed with curing agent in a 10:1 wt ratio (Sylgard 184 Silicone Elastomer Kit), as previously described by Peñaherrera et al.³⁰. Then, the mixture was placed under vacuum for 30 min to remove air bubbles, poured onto the ERmold and cured in an oven at 40 °C overnight (Figure 3). After curing, the PDMS replica was peeled off from the mold and holes for inlets and outlets of the channels were punched using a 1mm diameter biopsy puncher (Integra Miltex®Ted Pella, Inc). Finally, the replica was irreversibly bonded to a glass wafer after exposure to a high frequency generator (BD-10AS, Chicago) for 120s²⁹.

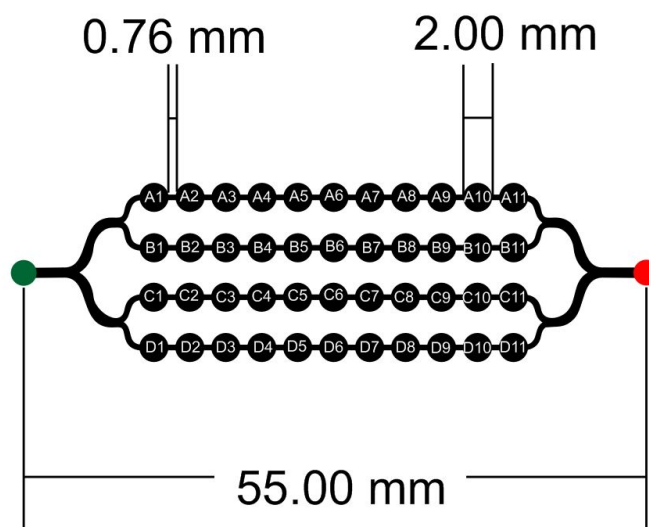


Figure 3 - Design of the microfluidic device. For breast cancer cells cultures. With four microchannels of 500 μm wide, eleven chambers in each of 1690 μm in width and a total internal volume of 150 μl . Each chamber has an alphanumeric code depending on the position. Inlet and outlet are represented by green and red respectively.

4.2.- Established cell line and cell culture

JIMT-1 cells ATCC 589 (DSMZ) were cultured in complete DMEM medium (Gibco), supplement with fetal calf serum heat-inactivated (FBS) 10% (w/v) (Gibco), L-glutamine 2 $\text{mmol}\cdot\text{L}^{-1}$ (Gibco), penicillin 100 $\text{units}\cdot\text{mL}^{-1}$, streptomycin 100 $\mu\text{g}\cdot\text{mL}^{-1}$ (Gibco) at 37 $^{\circ}\text{C}$ in an incubator with 5% CO_2 . Cells were resuspended with trypsin 0.50 $\text{mg}\cdot\text{mL}^{-1}$ and EDTA-4Na 0.2 $\text{mg}\cdot\text{mL}^{-1}$ (Gibco), and incubated at 37 $^{\circ}\text{C}$ for 3min. Trypsin was inactivated with FBS and cells were washed with phosphate buffer solution (PBS) (NaH_2PO_4 50 $\text{mmol}\cdot\text{L}^{-1}$, NaCl 300 $\text{mmol}\cdot\text{L}^{-1}$, (pH = 7.6) and centrifuged at 1200 rpm for 5 min. Finally, the cells were resuspended in the same complete DMEM medium. Before loading the cells, we pre-treated the microfluidic chips were cleaned using NaOH 0.1 $\text{mol}\cdot\text{L}$ for 1 hr, and then rinsed with 70 % ethanol and sterile water. Before cell seeding, chip was treated with poly-D-lysine hydrobromide 0.1 $\text{mg}\cdot\text{mL}$ (Sigma) sterile solution to improve cells attachment. The microdevice was incubated with poly-D-lysine solution for one hour at 37 $^{\circ}\text{C}$. The cells were loaded into the cell inlets of the chip with syringe pump (Adox), with 280

μLmin^{-1} flow rate at cell density of 1×10^6 cells ml^{-1} . Besides, cell culture assays were performed using the μ -Slide 8 wells- (Ibidi GmbH) according to the manufacturer's protocol.

4.3.- Cell viability (LC) analysis in Ibidi slides

We used the Live/Dead Cell Imaging Kit (Sigma) to evaluate cell viability in the Ibidi chip. In the Live/Dead assay, the viable cells are stained green with calcein, while the dead cells are stained red with propidium iodide. The cells were loaded into the Ibidi devices and evaluated cell viability at third, fourth, and fifth days; we used phosphate buffered saline (PBS, HyClone) to wash the culture chambers in the models for 1–3 min. Then, the cells were incubated with the Live/Dead Cell Imaging Kit for 15–30 min at 37 °C. Next, we used PBS again to wash out the reagent for 3–5 min and observed the culture chambers under a fluorescent microscope. Finally, cell viability was measured by assessing the percentage of green and red fluorescent cells related to the percentage of extension covered by the cells in the images.

4.4.- Autophagy activity (AG) analysis in Ibidi slides

We used the Autophagy Cell Imaging Kit (CYTO-ID) to evaluate cell spontaneous resistant in the Ibidi models. In the autophagy assay, the cells in autophagy are stained green, negative and positive controls were performed as recommended by the manufacturers' instructions (Enzo ENZ-51031-K200)³². The cells were loaded into the microfluidic devices, as described previously, and evaluated autophagy at one, third, fourth, and fifth days; we used phosphate buffered saline (PBS, HyClone) to wash the culture chambers in the models for 3 min. Then, the cells were incubated with the Autophagy Cell Imaging Kit for 30 min at 37 °C. Next, we used PBS again to wash out the reagent for 5 min and observed the culture chambers under a fluorescent microscope. Finally, autophagy was measured by assessing the percentage of green fluorescent cells related to the percentage of extension covered by the cells in the images.

4.5.- Apoptosis: Caspase-3 and -7 activity (AP) analyses in Ibidi slides

We used the caspase-3 and-7 Cell Imaging Kit (Invitrogen) to evaluate apoptosis (Utsumi, F., 2013) in Ibidi models. In caspase-3 and-7 assay, the apoptosis cells are stained green. The cells were loaded into the model as described previously and evaluated apoptosis activity at third, fourth, and fifth days; we used phosphate buffered saline (PBS, HyClone) to wash the culture chambers in the models for 1 - 3 min. Then, the cells were incubated with caspase-3 and -7 Cell Imaging Kit for 30 min at 37 °C. Next, we used PBS again to wash out the reagent for 3-5 min and observed the culture chambers under a fluorescent microscope. Finally, apoptosis activity was measured by assessing the percentage of green fluorescent cells related to the percentage of extension covered by the cells in the images.

4.6.- Caspase-independent cell death mode (PI) analysis in Ibidi slides

We used propidium iodide (PI) (Sigma-Aldrich) to evaluate death cells in Ibidi chip. PI assay death cells are stained red. Cells were loaded into the model as described previously and death cells were evaluated during fifth days; phosphate buffered saline was used (PBS, HyClone) to wash the culture chambers in the models for 1-3 min. Then, the cells were incubated with PI for 30 min at 37 °C. Next, we used PBS again to wash out the reagent for 3-5 min and observed the culture chambers under a fluorescent microscope. Finally, PI activity was measured by assessing the percentage of green fluorescent cells in all of the cells.

4.7.- Paclitaxel and doxorubicin drugs schematics and the evaluation of Live/Dead, Autophagy activity, Apoptosis and Caspase-independent cell death mode activity

For the drug schematics tests, the effects of paclitaxel (Sigma Aldrich) and doxorubicin (Sigma Aldrich) combined were studied (Holmes, F., 1996). First, JIMT-1, were loaded into the IBIDI chips, as described before, and 24 h later when the cells were adherent, we replaced the medium with fresh culture medium mixed with doxorubicin (DOX) concentrations of 0.01 μ M, Then, after 4 hours we

replaced the corresponding fresh culture medium mixed with paclitaxel(PAX) concentrations of 0.001 μM for 24 hours in order to evaluate the drugs effect; live imaging and biological characterization with different staining as described before was performed for the whole experiment.

4.8.- Paclitaxel drugs metronomic and the evaluation of Live/Dead, Autophagy activity, Apoptosis and Caspase-independent cell death mode activity.

For the drugs metronomic tests, the effects of paclitaxel (Sigma Aldrich) were studied(Lien, K., 2013). First, JIMT-1, were loaded into the IBIDI chips, as described before, and 24 h later when the cells were adherent, we replaced the medium with fresh culture medium mixed with paclitaxel concentrations of 0.001 μM . Then, every 24 hours for the following five days, we replaced the corresponding fresh culture medium mixed with paclitaxel concentrations of 0.001 μM . biological characterization with different staining as described before was performed for each day.

4.9.- Cell imaging and image analysis

Cell images for growth and development of BCC were obtained using the Olympus ScanR microscope. A 10x magnification was used, according with this each image have the dimension of 867x660 μm , with a conversion factor 0.64500 $\mu\text{m}/\text{pixel}$, and a final pixels per image 16 bit of 1346x1024. Olympus ScanR microscope allows the cultivation in controlled conditions of temperature, humidity and CO₂ %, at the same time as the image acquisition in real time using brightfield and fluorescence microscope. Image analysis was developed in Fiji: an open-source platform for biological-image analysis(Schindelin, J., 2012) which provides optimal tools for total cell area extension. A total number of 7500 images were analyzed with WEKA segmentation training on FIJI in order to measure total occupied area by cells. All the experiments were performed in triplicate. . All of the experiments were performed in triplicate, and the data are presented as the

mean \pm standard deviation (SD). A one-way analysis of variance (ANOVA) and Student's t-tests were used for comparisons of each group. P-values less than 0.05 were considered statistically significant and are indicated with asterisks (*).

In relation to specific objective 3, 4 and 5:

4.9.1.- data set Construction

data set: The images collected for the data set were taken in each biological step related to cellular growth and the use of different chemotherapeutic agents and drug schemes. A 20x magnification was used, according to this each image have the dimension of 433x330 μm , with a conversion factor 0.32250 $\mu\text{m}/\text{pixel}$, and a final pixels per image 16 bit of 1346x1024. Each brightfield image taken by the microscope was triplicated in the same position by different filters choosed to evidentiante the biological structure labeled with the correspondent fluorescence. For the H \ddot{o} chst filter we used an excitation filter 377/50 with an emission filter of 437-475 nm, for the propidium iodide filter we used an excitation filter 575/25 with an emission filter of 600-662 nm, and for autophagy and caspase we used an excitation filter 494/20 with and emission filter of 510-552 nm. Related to cellular growth, we collected 21873 cell images in total divided in five days of growthment. Related to chemotherapeutic drug schemes we collect 3839 cell images with paclitaxel treatment by five days. In the case of Paclitaxel and doxorubicin drugs schematics treatments we collect a total number of 15326 cell images.

Image preprocessing and labeling: The procedure of image pre-processing involve cropping all the images, by centering individual cells in a squared region of interest (ROI) via detecting cell contours with hough transform (Duda, R. O., 1972). Additionally, different image parameters need to be automatically adjusted. First, we converted the 16 bit image from the microscope with three sequential operations: scaling, taking an absolute value, conversion to an unsigned 8 bit type. Second, in order to provide normalized input to the network, we adjusted brightness and contrast in the brightfield images, and finally we enhanced edges

on the images by means of a Laplacian filter while still maintaining the structural aspect of the image. These pre-computations were implemented in Python using OpenCV (Open Source Computer Vision Library) framework, an open source computer vision and machine learning software library. Images in the data set were grouped in four different classes: live, dead, autophagy and apoptosis. Finally, three splits of the full data set were constructed to facilitate training and evaluation tasks: 80% of the samples are used for training, 10% for validation and 10% for testing, as suggested in most Deep Learning literature (Glassner, A., 2018, Goodfellow, I., 2016).

4.9.2.- Deep Neural Network for cell image classification

Neural Network: A Deep Convolutional Neural Network trained for classification on the constructed data set. We evaluate several state-of-the-art network architectures like VGG-19 (Simonyan, K., 2019), AlexNet (Krizhevsky, A., 2012), and Resnet (He, K., 2016). The network and the training loop were implemented using Pytorch framework and Python.

Equipment: A notebook was used for the creation of the data set. Training of the CNN was performed on an Intel Xeon server equipped with two Graphics Processing Unit (GPU) Nvidia Titan Xp and 32Gb of RAM.

5.- Results

Due to the importance of generating a database of representative images of the biological behaviour of BCC with different staining to evaluate growth related to cell death modes a LOC microfluidic system (Figure 3) and Ibidi slides was used. The microfluidic system allowed the tracking and evaluation of the growth and development of breast cancer cells inside of de LOC. BCC characterization assays are an *in vitro* method based on the intrinsic property of self-renewal capacity of these kind of cells. In order to analyse the growth and development of JIMT-1 within the microdevices, the concentrations of cells seeded in LOC were measured and the flow rate for the syringe pump was kept constant throughout the experiment. By

measuring the total number of cells inside the chambers of LOC microdevices it was observed that the concentrations of cells were not effective. This lack of effectiveness was due to the fact that the cells were not able to form a high and reproducible number of cells in the chambers, with a non homogeneous distribution observed between the different chambers. This phenomenon of not homogeneous distribution was represented with a smaller number of cells in the chambers closest to the inlet in comparison to the ones located near the outlet (Figure 4). Without a differential distribution within the channels and chambers.

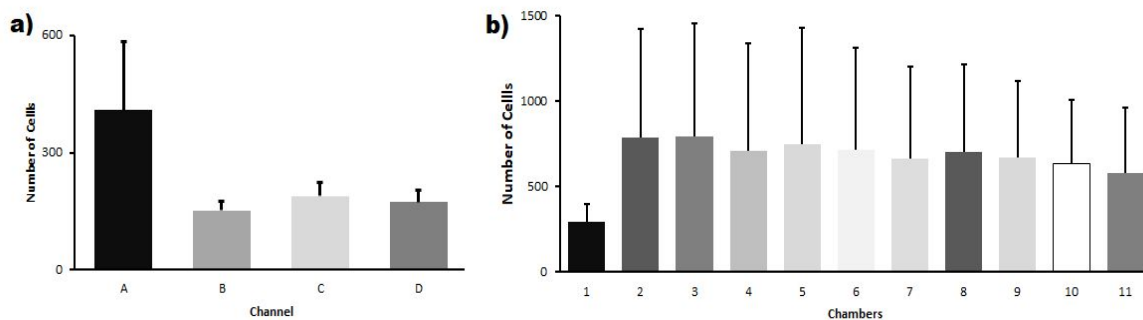


Figure 4 - Number of cells development depending on the microdevice position, (a) inside of the channels, (b) inside of the chambers.

5.1 Tracking the growth breast cancer cells in PDMS chips

Concomitant to cell growth of JIMT-1 in the LOC devices, our results show the monitoring for the following four days. It was observed that some cells started to generate protrusions after five hours after loaded in the chambers of the device (Figure 5b, red arrow). And after 9 hours, they started to divide (Figure 5c). It was noticed that the BCC presented different growth rates independently of the initial cell concentration.

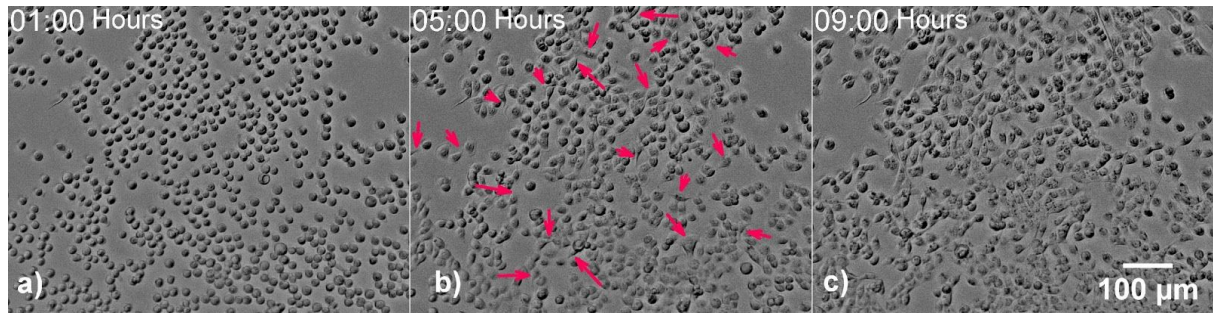


Figure 5 - a) BCC after one hour of seeding with cells Live imaging inside of the chambers of microfluidic device for 9 hours (c). Red arrows (b) show the protrusions of cells after 5 hours approximately. Scale bar: 100 μm

It was noticed that the BCC presented different growth rates independently of the initial cell concentration (Figure 6). The growth rate analysis of JIMT-1 as a function of the initial seeding concentration was defined by the area occupied by cells inside the chambers, analysed over five days (Figure 6). After five days of cells growth we observed that the BCC blocked the channels between wells preventing the feeding of the whole chip.

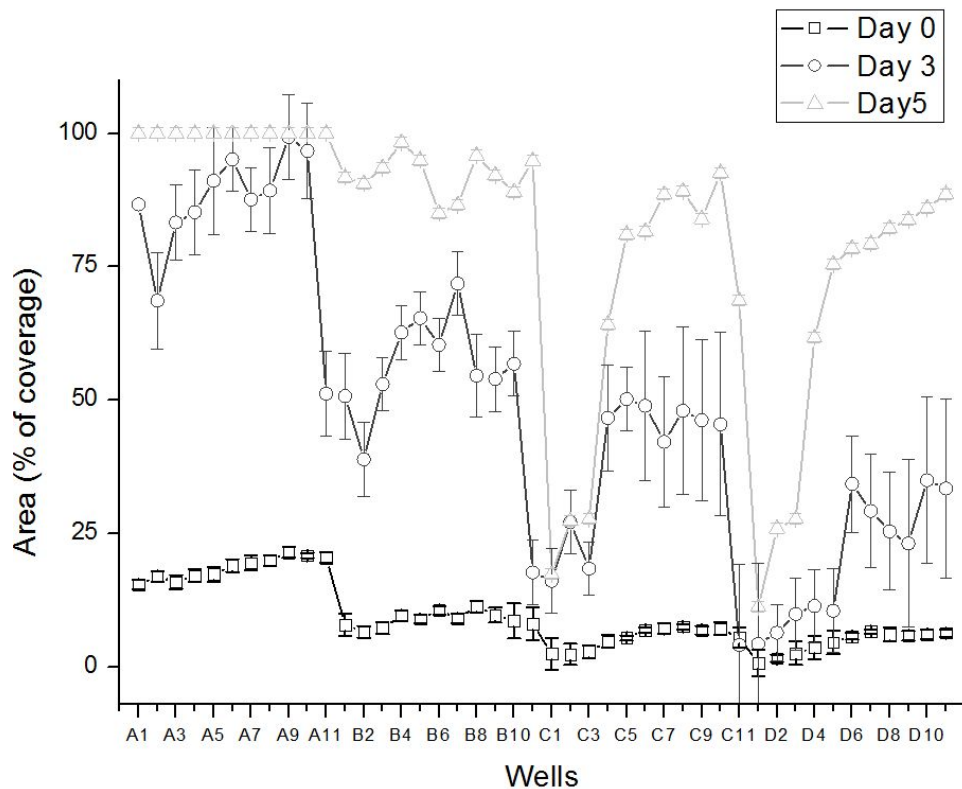


Figure 6 - Area of cells depending on the microdevice position, in different days.

5.2 Tracking the growth breast cancer cells in Ibidi chips (IC).

In order to complement the database with images of BCC cultured *in vitro* with different methods we use Ibidi slides. We used a chambered coverslip with 8 independent wells and a non-removable polymer coverslip-bottom which allowed the tracking and evaluation of the development of breast cancer cells during five days. This setup tolerates live cell imaging over extended time periods and provide high optical quality with a total growth area per well of 1.0 cm². We then applied different schematic drugs for evaluating the efficacy of therapeutic agents with the associated fluorescence labeling employing low volume of reagents. We analyze the development and characterization of JIMT-1 within the chambers of the Ibidi slides. We measure the percentage of area covered by the fluorescence exhibited by the different biological behaviour of cell viability (LV), apoptosis activity by caspases 3 and 7 (AP), autophagy activity (AG), caspase-independent cell death process (PI) over the five days (Figure 7).

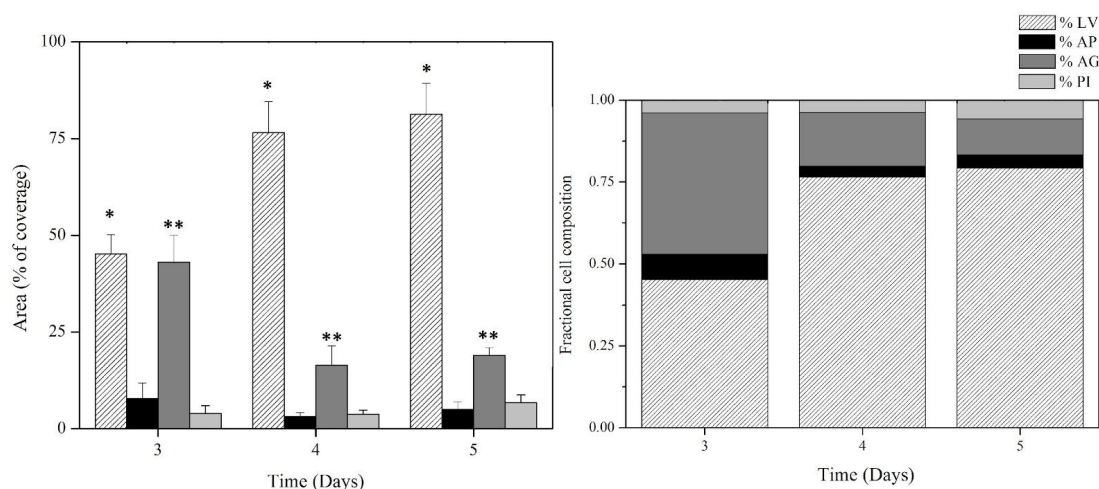


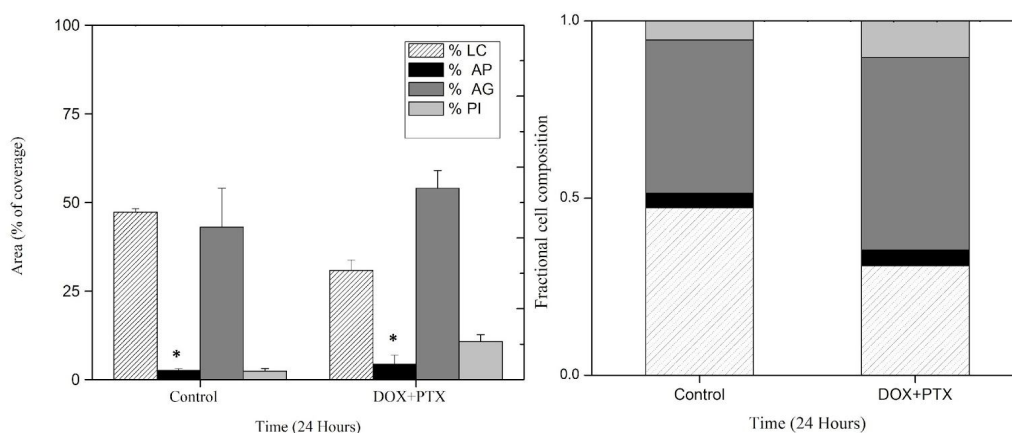
Figure 7 - Bar graph showing characterization of cells. Area of cells after characterization with stainings for 5 days.

It was observed significant differences in the percentage of LC and AG. Percentage of live cells increased for five days (Figure 7). In contrast, cells in autophagy showed high percentage of area at third day and decreasing a long of the fifth day. The presence of cell death caspase dependent modes (AP) was higher than the independent cell death modes (PI) on the third day. Correlation that was inverted at the end of the study in the fifth day.

5.3 Effect of Paclitaxel and doxorubicin drugs schematics and the evaluation of LC, AG, PI and AP.

The database was complemented with images of JIMT-1 cultured *in vitro* treated with anti-cancer drugs. The effect of the therapeutic agents: doxorubicin and paclitaxel on the percentage area shown by the four different biological behaviour, was studied. In all cases the percentage of fluorescent area covered is related to the entire cell population of the sample. First of all, it was studied the doxorubicin(DOX) effects. BCC samples were incubated for four hours with the drug with 0.01 μM of concentration. We observed that the percentage of fluorescent area covered by Apoptosis caspase cell death mode (AP) was significantly higher in the samples exposed to the DOX respect to the control (Figure 8). In addition, our results (Figure 8A) indicate that the cell viability was not reduced significantly (live cells), also it was evidenced a slight increase in the area of the autophagy process in comparison to the control.

8A)



8B)

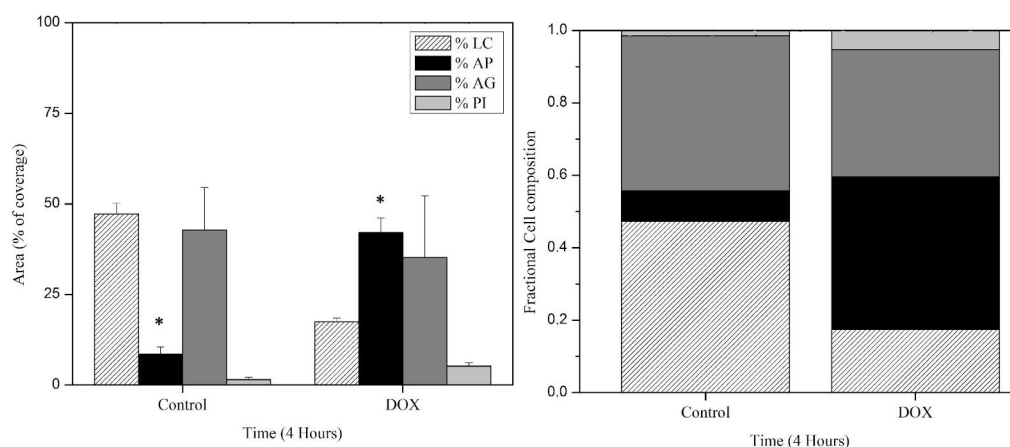


Figure 8.- Percentage of fluorescent area covered related to the entire cell population of the control sample and drug schematic treated sample. 8A: BCC samples were incubated for four hours with DOX 0.01 μM of concentration. 8B: BCC samples after DOX treatment incubated twenty-four hours with PAX 0.001 μM

Afterwards, paclitaxel effect on the percentage area shown by the four different biological behaviour was evaluated on samples that previously were treated with DOX.

It can be seen that there is an inversely proportional correlate of the biological behaviour studied in the treated sample. In comparison with the control sample, the area of activity of the processes: PI, AG and AP there is no significantly different in comparison to control. However, the LC percentage area is lower extended at the end of the treatment with the additive schedule drugs (Figure 8B).

5.4 Effect of Paclitaxel drug in low-dose metronomic (LDM) and the evaluation of Live/Dead, Autophagy activity, Apoptosis and Caspase-independent cell death mode activity.

Another treatment to complement database images was paclitaxel drug in LDM application on JIMT-1 cultured *in vitro*. The correspondent analysis of the percentage

area shown by the four different biological behaviour, was performed. In all cases the percentage of fluorescent area covered is related to the entire cell population of the sample. Paclitaxel was tested in very low concentrations for a period of five days. We observed that this drug had a great effect on LC (Figure 9), causing a decrease in the area of the treated cells with respect to the control (Figure 9). As the days of treatment increase, an increase in the percentage of AP activity area can be observed. While the percentage of AG process area remains relatively constant as well as PI which represent the independent cell death of caspase.

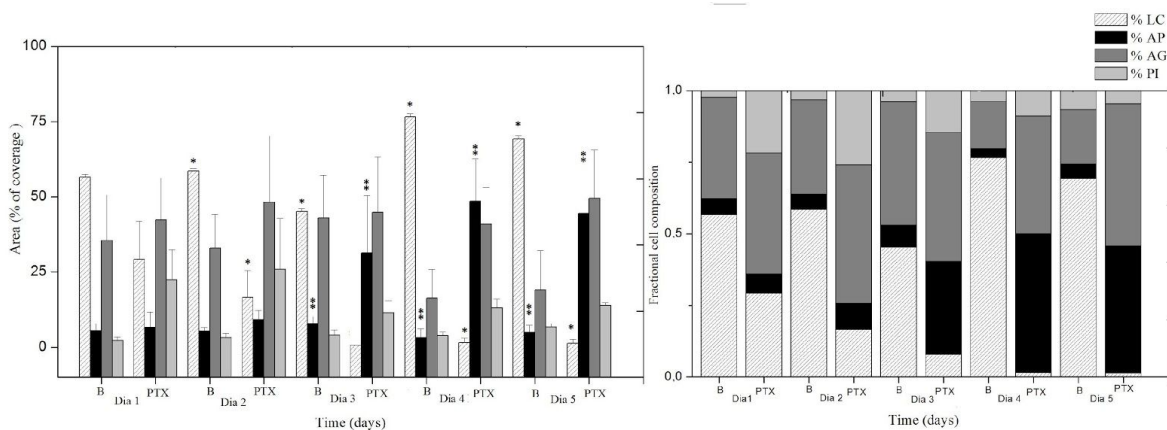


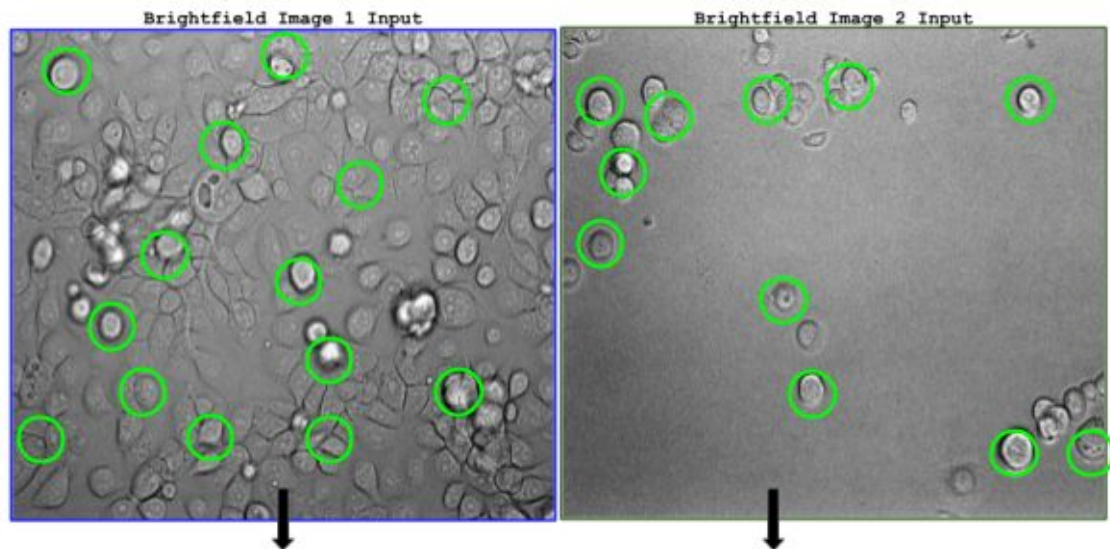
Figure 9- Percentage of fluorescent area covered related to the entire cell population of the control sample (B) and low-dose metronomic treated sample (PTX).

5.5 Segmentation process to individualize cells and labeling with the corresponden biological state

The full set of images generated with the previous steps undergo a necessary curation process in order to organize the final data set. Our data set fully consists on breast cancer cells JIMT-1. In order to train neural networks to automatically classify them it is necessary to detect and segment individual cells from the brightfield images. In addition to the segmentation, each individual cell should be tagged with a label indicating the classification category it belongs to (i.e. live/dead), obtained from the associated staining image. We now summarize the analytic data pipeline in the following steps:

Image conversion

Import images, 8 bit resampling, Laplacian filter, Cell detection and labeling



```
[ ] im16 = cv2.imread(ruta, cv2.IMREAD_ANYCOLOR | cv2.IMREAD_ANYDEPTH).
im8 = cv2.convertScaleAbs(im16, alpha=255/im16.max(), beta=0.)

[ ] img = cv2.Laplacian(img,cv2.CV_64F,ksize=25).

[ ] cell_recognition = cv2.HoughCircles(img,cv2.HOUGH_GRADIENT,1,30,param1=25,param2=30,minRadius=25,maxRadius=35)

[ ] #LOOP
for circle in cell_recognition:
    # Define x, y and radius
    x = circle[0]
    y = circle[1]
    r = circle[2]

    # Cut the rectangular selection and save
    cv2.circle(circles,(x,y), r, (0,255,0),2)
    result = img[y-r:y+r,x-r:x+r]
    cv2.imwrite('cell_process_day\save_{}.png'.format(counter),result)
```

Figure 10 - Pipeline showing inputs brightfield images 1 and 2 in 16 bit and the subsequent steps automatically applied by our image filters: resample the image to 8 bit (from the original 16 bit), laplacian filter. The cell recognition function we developed is schematic represented by circles on the image.

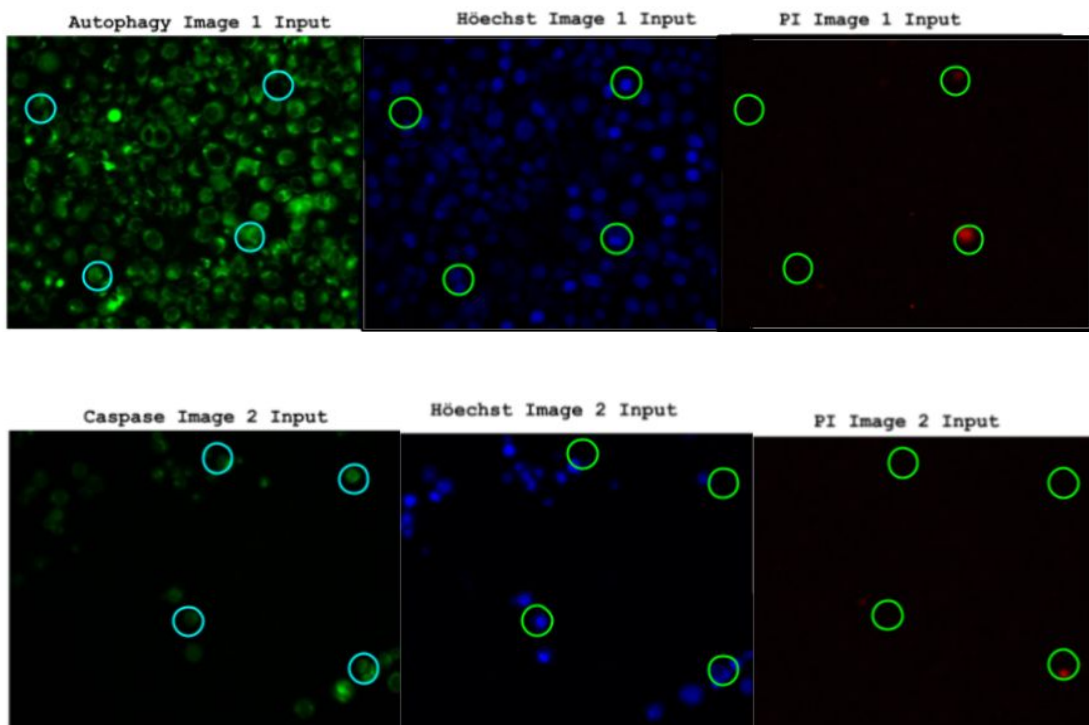
Pre-processing the raw images provided by the microscope is a crucial step in our classification pipeline. To this task, we used one of the most standard libraries in the

image processing field: OpenCV². The original raw brightfield images were encoded using a 16 bit representation. In order to apply some of the pre-coded image filters in OpenCV, we first needed to convert them to an 8 bit representation. Then, we identified each cell by means of the by Hough Circles transform (Yuen, HK., 1990) . This algorithm automatically finds circular shapes represented mathematically as equation 1 evidence:

$$(x - x_0)^2 + (y - y_0)^2 = r^2$$

Equation 1 - Equation used by the algorithm to find circular shapes on bright field images.

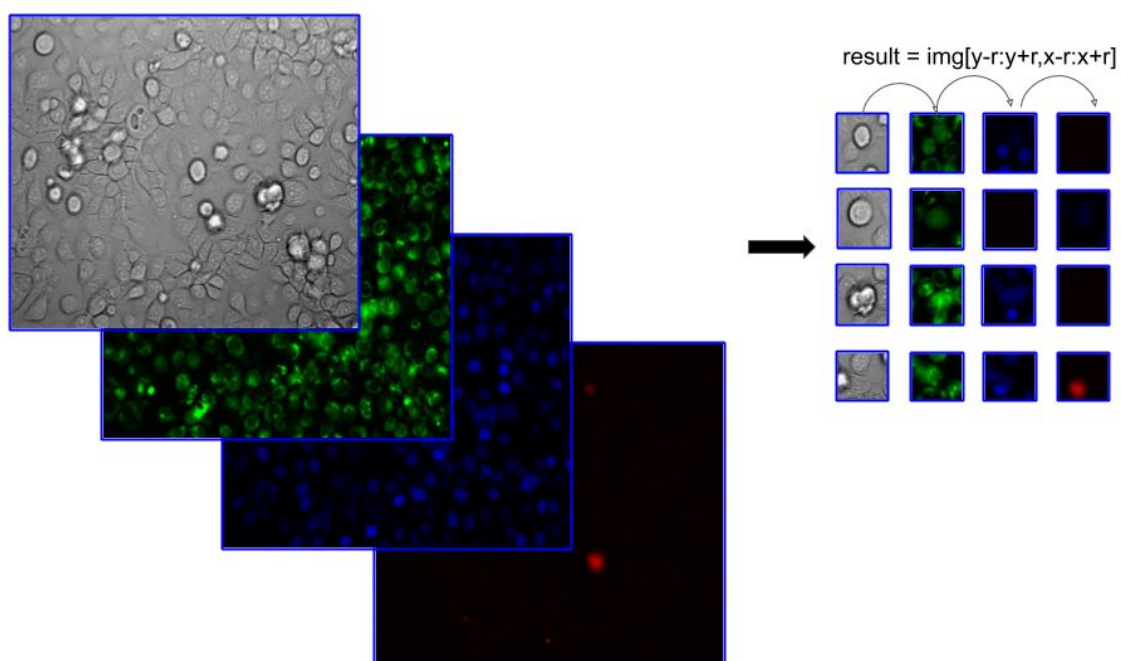
where (x_0, y_0) are the 2D coordinates of the center, and r is the radius of the circle. We assist the function by specifying the minimum and maximum radius range: $minRadius = 25$ and $maxRadius = 35$. We experimentally found this range to be representative of the size of most cells in our data set. From each raw image we obtained the position coordinates of each cell in the brightfield image (Figure 10).



² Open Source Computer Vision Library <https://opencv.org>

Figure 11 - Schematic representation of corresponding fluorescent images with the same detected circle region identifying each recognized cell. Up) Left: autophagy process fluorescence, middle: höchst nuclear fluorescence, right: dead cell with propidium iodide fluorescence. Down) Left: caspase activity fluorescence, middle: höchst nuclear fluorescence, right: dead cells with propidium iodide fluorescence.

A)



B)

```
[ ] #LOOP
    for circle in cell_recognition:
        # Define x, y and radius
        x = circle[0]
        y = circle[1]
        r = circle[2]

        # Cut the rectangular selection and save
        cv2.circle(circles,(x,y), r, (0,255,0),2)
        result = img[y-r:y+r,x-r:x+r]
        cv2.imwrite('cell_process_day\save_{}.png'.format(counter),result)
```

Figure 12 - Schematic representation showing the way we cut the same region after the circle detection step identifying cells over the brightfield. A) Green fluorescence: autophagy activity, blue fluorescence: Hoechst nuclear staining, red fluorescence: dead cell with propidium iodide fluorescence. B) Corresponding cutting code in python.

Given the circle detection identifying each cell in the brightfield, we then segment them on fluorescence labeled (Figure 11) and cut the same region over the corresponding fluorescence information (Figure 12 and 13). We had two green fluorescence labeled: caspase and autophagy activity, blue fluorescence that correspond with Hoechst, a nuclear staining, and red fluorescence that involve dead cells with propidium iodide.

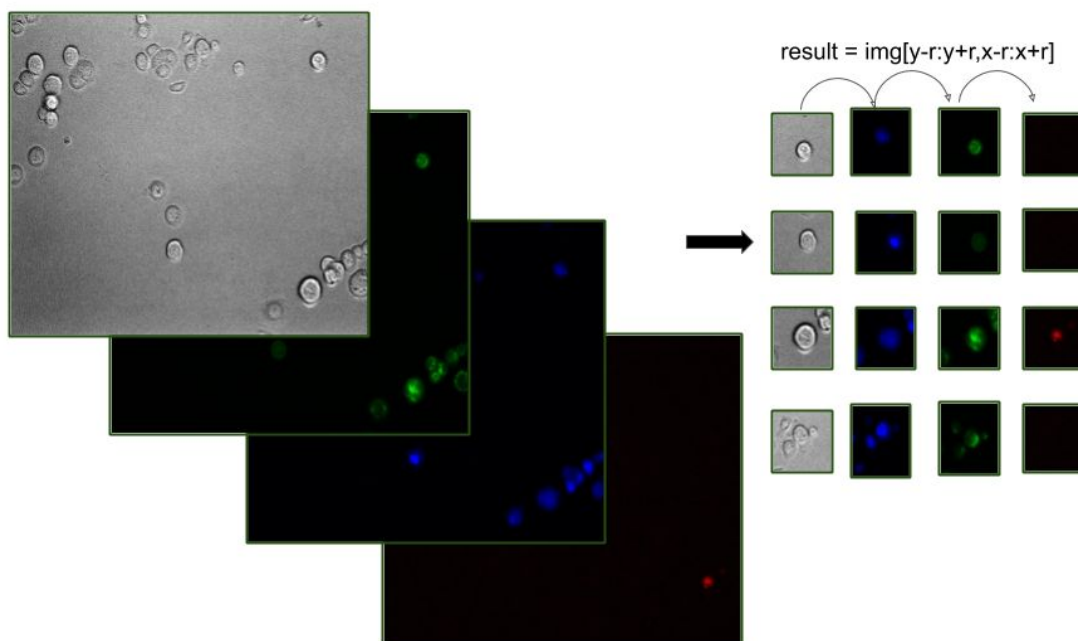


Figure 13 - Schematic representation of region cuts after the circle detection step, identifying each cell in the brightfield. We cut it along with its corresponding fluorescence information. Green fluorescence: caspase activity, blue fluorescence: hoechst nuclear staining, red fluorescence: dead cells with propidium iodide.

Summarizing, with the circle detection function we identify each cell in the brightfield image. From each raw image we obtained and saved in a text document the position coordinates of each segmented cell segmented, it coordinates x, y and the radius. We also saved the adjusted brightfield image and the corresponding region over the

fluorescence channel. Furthermore, we assigned each cell a unique integer identifier and saved the associated fluorescence information (detailed on the following steps).

Detecting cells by fitting circle shapes over the image has both, advantages and disadvantages. For some cases, the circular detection was successful. However, there were cases where the cells generate extensions of their membrane which causes the circular detection does not encircle the entire cell. Then, our automatic detector only retrieves the area around the cell nucleus (Figure 14).

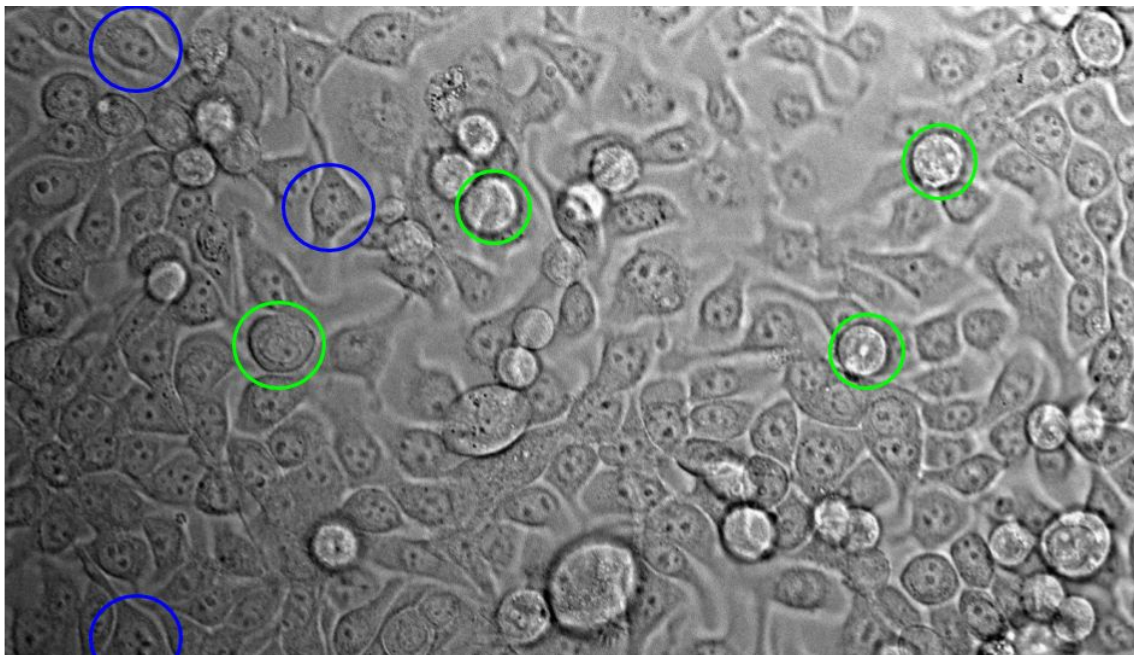
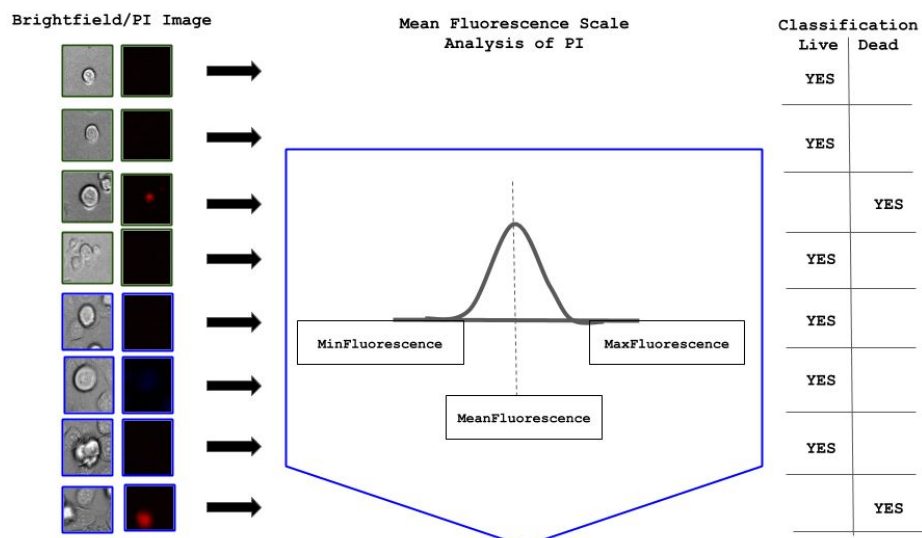


Figure 14 - Brightfield image of JIMT1 where we observed green circles that shown successful circular detection of cells. And blue circles where detection does not encircle the entire cell.

Live/Dead cell labeling




```
[ ] info_pixels = []
    # For each PI image output
    for output_PI in list_of_images:
        # Decide based on fluorescence Live or Dead
        mean_of_pixels = np.mean(output_PI)
        max_of_pixels = np.max(output_PI)
        min_of_pixels = np.min(output_PI)

        info_pixels.append([max_of_pixels,min_of_pixels,mean_of_pixels])

        if(mean_of_pixels > 415):
            #is Dead
            info_vm.append(0)
        else:
            #is Live
            info_vm.append(1)

    print ('mean fluorescence', mean_of_pixels)
    print('maximum fluorescence', max_of_pixels)
    print('minimum fluorescence', min_of_pixels)
    print ('DEAD is labeled with 0', 'LIVE is labeled with 1')
```

Figure 15 - Analyzing information of pixel intensities from each propidium iodide fluorescence. Approximate distribution of the fluorescence values and the assigned labels each cell based on the mean fluorescence for live or dead.

In order to associate each cell in our data set with the labeling information (cell viability, autophagy and caspase activity), we jointly processed each brightfield image with the fluorescence images. We analyzed the pixel intensities on those images to obtain a ground truth (GT) live-dead labeling useful for training our classifiers.

One key aspect to succeed when training a classifier is to have reliable labels associated with each training image. In our case, we choose a threshold value to determine if an individual cell is dead given the propidium iodide fluorescence. In order to perform this task, we took as input the fluorescence pixel information obtained from PI labeled images. Although propidium iodide has the characteristic of only entering the cell when its membrane has compromised the fluorescence spectrum, its emissions are not uniform and may overlap and occupy more than one cell diameter. This generated a scenario where a clear criterion to properly determine the labeling threshold was needed.

To find a solution, we observed pixel intensities across many samples in our data set. On the one hand, choosing a very high threshold (high fluorescence values)

would assure us more certainty in the cell images labeled as dead, but possibly we would be labeling as alive many images which are very far from the low fluorescence values indicating dead signs. On the other hand, the opposite effect would be observed if choosing a very low threshold. Our goal is to come up with a threshold value which is able to split images into live/dead categories, while minimizing the number of samples lying close to the frontier. For this reason we decided to compute and use as a threshold the average fluorescence value among the cells in our data set. First, we use *maximum* function to find the element-wise maximum for 1718 cells in our data set. Then, we compute the *minimum* to find the corresponding element-wise minimum. Finally we complement both parameters with the *mean fluorescence*. Notice we compute these values directly from the raw fluorescence images, without any pre-scaling. The aforementioned vector operations over images were performed using Numpy library³. We finally label each cell based on the mean fluorescence for live or dead. In order to decide the final value to automatically classify cells, we computed the average of the mean fluorescence over five days. If, for a given cell image the mean fluorescence of pixels in its surrounding area is higher than the pre-computed mean, then the image is labeled with 0 (zero), meaning the cell is dead. On the contrary, if the computed value is below the global mean, the cell is labeled with 1 (one) which means the cell is alive (Figure 15). In order to determine the main criterion to ensure the effectiveness of the live/dead classification a statistical sample analysis was performed. The methodology to validate this indicator is as follows: we first selected fifty aleatory brightfield and PI images from each day of treatment with paclitaxel drug in LDM application on JIMT-1 cultured *in vitro* (Table 2). As shown in table 2, from each of the cells detected we extracted their fluorescence values: maximum and minimum, and the correspondent mean.

As evidenced in the Table 2, regardless of the number of cells detected, the *min*, *max* and *mean* values were relatively similar, indicating some trustworthy degree of calibration in the microscope output for the fluorescence range values. The maximum fluorescence remained close to 800 units, and the minimum fluorescence

³ Numpy library: <https://docs.scipy.org/doc/numpy/index.html>

surrounded 30 units for all the analyzed images. Furthermore, this is a strong indicator that the process of death and staining with propidium iodide fluorescence is not modified despite being on different days of growth and treatment.

In our experiments, the selected threshold value is 414.72. Consequently, all cells recognized from the data set that show a higher mean fluorescence value than 414.72 are labeled as dead. Any other cell below that threshold is considered to be alive (Figure 15).

Drug_day_staining	Images	Cells detected	Mean_MaxFluorescence	Mean_MinFluorescence	Mean_MeanFluorescence
Taxol_1d_PI	50	428	823.5	30.98	418.32
Taxol_2d_PI	50	396	830.19	31.04	423.58
Taxol_3d_PI	50	467	791.87	31.01	408.56
Taxol_4d_PI	50	325	840.04	31.22	422.03
Taxol_5d_PI	50	102	787.05	31.31	401.12

Table 2 - Fluorescence information from the fifty selected images from each day of treatment with paclitaxel drug in LDM application on JIMT-1 cultured *in vitro*. The average value of the mean fluorescence founded over the five days analysis was 414.72.

5.6 Convolutional Neural Network Training

data set partitions

In order to learn a model for classification, we profit from Convolutional Neural Networks (CNN) (LeCun, Y., 2015). We trained CNNs in a supervised fashion, which means using pairs of labeled inputs to fit a model able to generalize to unseen samples and to predict the output labels for new data. Our predictive model produces binary outputs, a classification between two categories: live or dead.

In order to evaluate the network power under different scenarios we built three different data set partitions. Then, we describe a preliminary CNN architecture

evaluation and introduce Deep Learning concepts. Finally, we demonstrate the performance of a state-of-the-art network called SqueezeNet over some of our data set partitions. Since SqueezeNet architecture gave us the best results.

We report results and metrics from the performance of this network. :

- *celldata_mixed* containing cell images with and without drugs from different days of growthment,
- *celldata_livedead* containing cell images without drugs,
- *celldata_doxotaxol* with cell images with schematic therapeutic drugs of doxorubicin and taxol.

Description of the data sets metadata(their labeling characteristics, and number of cell images obtained):

- *celldata_mixed* contains cell images from 4 different scenarios of acquisition: 1) growthment from 3rd to 5th day without drugs, 2) four hours of treatment with doxorubicin, 3) schematic therapeutic treatment of doxorubicin and paclitaxel during 28 h, and 4) metronomic therapeutic scheme that imply low dose of paclitaxel during five days.

From each one, we detail the number of brightfield images used, number of individual segmented cell images and their corresponding labeling.

Growthment from 3rd to 5th day without drugs cell images: we process 747 brightfield images chosen between the 3rd and 5th day of cultivation (Table 3). We observed that images are in sharp focus in major amount when the cell line constitute the monolayer at the 5th day, while at the beginning of cell culture they are mostly out of focus. Still, blurred images were included as an additional source of variability that may benefit the training.

Day	Brightfield Images	Cells detected	Live	Dead
3rd	172	1708	1199	509
4th	275	1220	887	333
5th	300	846	564	282

Table 3 - Brightfield images with cells from 3rd, 4th and 5th day of growthment detected by programming code with Hough Circles transform and labeled in live and dead based on mean fluorescence value of PI.

With our automatic cell detection method we identified a total of 3774 cells, of which 70.2% correspond to live label (2650 cells).

Four hours of treatment with doxorubicin cell images: The brightfield images were selected based on the fact that each of them have their corresponding fluorescence used in this Thesis. This imply mandatory PI, but also AG, AP and Höechst, because in this way we made sure that we had the complementary fluorescence information for future analysis. We perform an analysis of 142 brightfield images of JIMT-1 treated only with 4hr of doxorubicin (Table 4). We detected 1062 cells, of which 70.6% correspond to live label (750 cells).

Drug_time	Brightfield Images	Cells detected	Live	Dead
Dox_4h	142	1062	750	312

Table 4 - Brightfield images with cells treated four hours with doxorubicin detected by programming code with Hough Circles transform and labeled in live and dead based on mean fluorescence value of PI.

Schematic therapeutic treatment of doxorubicin and paclitaxel during 28h cell images: We processed a total 2052 brightfield images corresponding to breast cancer cells exposed to schematic dose of doxorubicin 4hr plus taxol 24 h treatment, with the correspondent PI fluorescence (Table 5).

Drug_time	Brightfield Images	Cells detected	Live	Dead
Dox_4h_Tax_24h	2052	6096	4392	1704

Table 5 - Brightfield images with cells treated four hours with doxorubicin following twenty four hours of taxol, computed using Hough Circles transform and labeled in live and dead based on mean fluorescence value of PI.

We cut and labeled a total number of 6096 cell images. Live cells represent a 72% of the total (4392 cells).

Metronomic therapeutic scheme that imply low dose of paclitaxel during five days: Quantity difference of brightfield images from each day is biased in view of the fact that there are blurred features present and absence of monolayer in the beginning of the breast cancer cell line growth. Furthermore, this situation is enhanced because taxol effect favours circular shape and floating conditions according to the therapeutic effects (Figure 16).

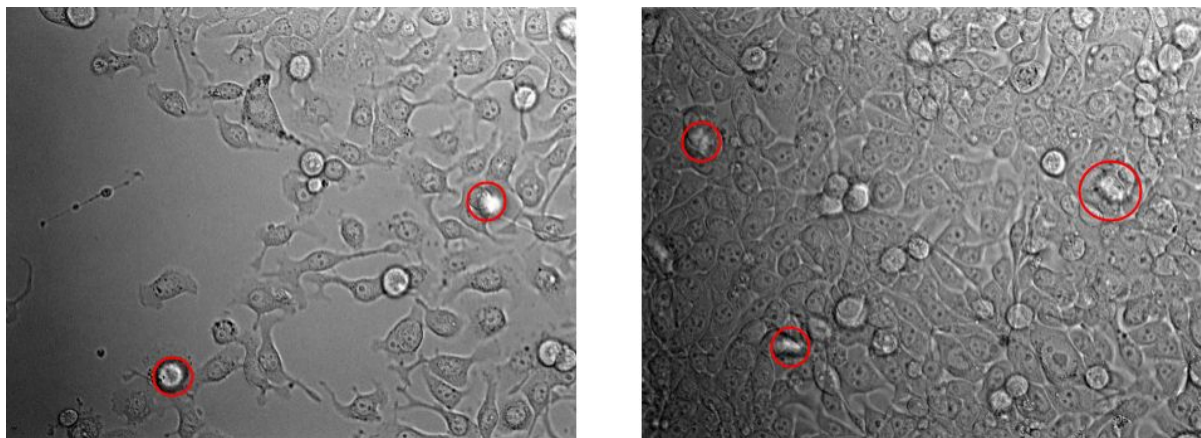


Figure 16 - Brightfield images of JIMT-1 with red circles showing blurred cells. On the left we observe absence of monolayer on the 3rd day of cellular growth. While, on the right we observe presence of monolayer on the 5th day of cellular growth.

We analyzed 651 brightfield images and obtained a total number of 3839 cell images segmented, labeled, and cropped (Table 6), among which 2616 were classified with live label (68%).

Scheme_Drug_day	Brightfield Images	Cells detected	Live	Dead
Metronomic_Tax_1d	134	1390	946	444
Metronomic_Tax_2d	182	546	377	169
Metronomic_Tax_3d	173	771	537	234
Metronomic_Tax_4d	214	915	609	306
Metronomic_Tax_5d	118	217	147	70

Table 6 - Brightfield images with cells treated by low-dose metronomic taxol, detected by programming code with Hough Circles transform and labeled in Live and Dead based on mean fluorescence value of PI.

- *celldata_livedead* contains cell images without drugs. We analyzed all the brightfield cell images without drug treatment available and we compiled a data set with a 18099 total live cell images, and 6781 total dead cell images (Table 7).

Condition	Brightfield Images	Cells detected	Live	Dead
Growth	1784	24880	18099	6781

Table 7 - Brightfield images with cells from 3rd, 4th and 5th day of growthment detected by programming code with Hough Circles transform and labeled in live and dead based on mean fluorescence value of PI.

- *celldata_doxotaxol* contains cell images with schematic therapeutic drugs of doxorubicin and taxol. We analyzed all the brightfield cell images under this specific drug treatment available and we reach compose a data set with was composed with a 8168 total live cell images, and 3200 total dead cell images (Table 8).

Drug_time	Brightfield Images	Cells detected	Live	Dead
Dox_4h_Tax_24h	3252	11368	8168	3200

Table 8 - Brightfield images with cells treated four hours with doxorubicin following twenty four hours of taxol, computed using Hough Circles transform and labeled in live and dead based on mean fluorescence value of PI.

Preliminary training configurations

In order to test the potential of the CNN to classify this type of data, we first perform a preliminary evaluation using several well known CNNs architectures like VGG and SqueezeNet, ResNet. In order to train the parameters of this network, we used our *celldata_mixed* data set, which contains cell images from the different scenarios of acquisition.

Networks are composed of many operations, each of which was designed to perform particular tasks. The choice and arrangements of the operations is called the architecture. The basis of convolutional neural networks consists on function that applies the same local linear function called kernel to every local context in a source tensor.

We evaluate Resnet 18, VGG and SqueezeNet to test potential deep neural network to classify this type of data. CNNs takes as input a set of brightfield images, and outputs classification labels: 0 and 1 (dead and live respectively). When loading the images, we applied a grayscale transformation, and resized images to 64x64. We further perform data augmentation (artificial new training samples) by applying random vertical and horizontal flips and random 90 degrees angle rotation. In order to optimize the CNN parameters we used an optimizer, that means, a specific algorithm that tunes the network parameters to optimize them and minimize the classification loss function (see below). In this setup we used Stochastic Gradient Descent (SGD). To accelerate the parameters adjustment we profit from transfer

learning technique (Goodfellow, I., 2016) which allowed us to start training from a pre-trained network over ImageNet⁴.

We train the model to learn how to predict cell states by feeding it with the labeled samples in our data set. This process is organized in iterative steps called epochs. During each epoch, the neural network is presented with all the training samples in our data set. For this preliminary test, we trained our CNNs over a short timeframe (25 epochs) in order to quickly evaluate several architectures. Within each epoch, the training checks the prediction performance by comparing the input labels in the data set with the predicted ones. In the deep learning literature, the error function used to compare labels is called loss function. In our setup, we compute Binary Cross Entropy (BCE) with logits loss defined as shown in Equation 2:

$$l_n = - [y_n \cdot \log p(x_n) + (1 - y_n) \cdot \log(1 - p(x_n))],$$

Equation 2 - Binary Cross Entropy (BCE) with logits loss.

where y is the label (1 for live, 0 for dead), and $p(y)$ is the predicted probability of the cell being alive for all n input points. Intuitively, the function tells us that for each live cell ($y = 1$), it adds $\log(p(y))$ to the total loss, that is, the log probability of it being alive. Conversely, it adds $\log(1 - p(y))$, that is, the log probability of it being dead for each dead-labeled image ($y = 0$) (Goodfellow, I., 2016). Therefore, the loss function penalizes big differences between ground truth and the predicted labels (accurate predictions result in lower loss value).

In our setup, we deal with a heavily imbalanced training data set, that is, different number of training samples for each label. This is mainly due to the fact that most cells in our raw data sets correspond to live states, with or without drug treatment. Therefore, naively using BCE loss would strongly bias the network towards positive responses, labeling most input images as alive. To counterbalance, each class is individually weighted with values inversely proportional to the number of samples for each class in the training data set. For simplicity, we omit from this formulation the

⁴ Extracted from <http://www.image-net.org/>

class weights, but the full weighted loss formulation can be found in descriptions made by Goodfellow, I., 2016.

Finally, the last key ingredient we have to mention is the learning rate, an hyperparameter controlling the speed at which the network parameters are adjusted (Glassner, A., 2018). In our implementation we experimented with several learning rates, and choose to report results for a learning rate of 0.00001.

Since this first experiment was only performed for the sake of validating the implementation and selecting the best neural architecture, we only worked with a binary data set split, that is training and validation. The training part represents 75% of the total number of cell images, and the validation comprises the remaining 25%. In total , we used 3000 individual cell images for training. Our validation data set is composed of 800 images and where only used for adjusting the hyperparameters and evaluating the training performance.

Automatic breast cancer cell classification with CNNs

From the aforementioned preliminary tests on several network architectures, the one model that outperformed all the others on automatic breast cancer cell classification was SqueezeNet (Forrest, N. et al, 2017). Therefore, following results and metrics are all reported over this architecture. We now show a number of experiments over two different data set splits and provide evidence of the morphological cues power in cell brightfields to perform automatic classification in live/dead states.

SqueezeNet architecture

The CNN was built according to the SqueezeNet. The topology of the network is shown in Figure 17.

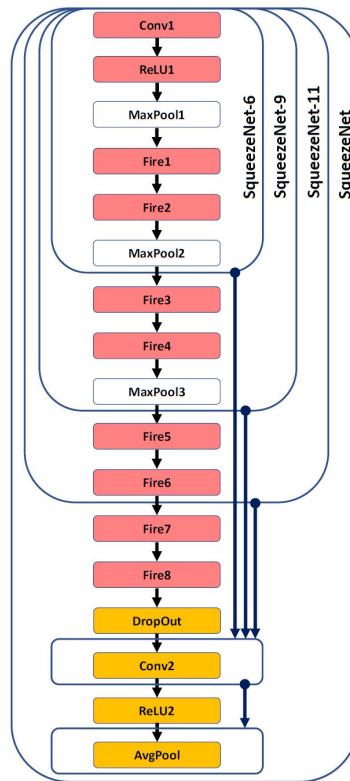


Figure 17 - The SqueezeNet architecture ⁵

The network consists of several convolutional layers, one squeeze layer and two expand layers. The first layer was modified to work with a one channel image input. From the original 1000 Image net classes, last layer was also adapted to classify the cells into two different classes: live and dead. The input image resolution was set to 224x224 pixels and the activation function used was ReLU.

For training the network we used the following configuration:

1. Optimizer: "Adam";
2. Learning rate: 0.00001;
3. Epochs: 500
4. Dropout: 0.5
5. Batch size: 4.

⁵ Extracted from DOI: 10.5220/0007484205560563

Loss function

In our setup, we compute Binary Cross Entropy (BCE) which has been already described in Section *Preliminary training configurations*.

Data process

When loading images before training the network, we applied a grayscale transformation to discard unused channels from the original images. We also perform , data augmentation in the form of random vertical and horizontal flips, and random 90 degrees rotation. Furthermore, we applied a color jitter transformation which randomly modifies brightness and contrast parameters up to 10%.

Metrics

We choose to evaluate our deep learning model with the following metrics: balanced accuracy score, F1-score, confusion matrix and Receiver Operating Characteristics curve (ROC).

Previously, is necessary to define some concepts related to metrics analyzed. True Positive (TP) are the dead cells when the actual class of the data point was 0 (true) and the predicted is also 0 (true). On the other hand, False Negative (FN) are the dead cells when the actual class of the data point was 0 (true) but predicted like live, it means the actual class of the data point was 1(false).

True Negatives(TN) are the live cells when the actual class of the data point was 1(false) and the prediction is also live, it means 1(false). In opposition False Positive (FP) are the live cells with actual class of the data point was 1(false) predicted as dead cells(class 0) incorrectly.

Accuracy (A) is described in Equation 3, and it is a general measure of how often the network prediction is correct. It is computed by the sum of the ground truth dead cells classified as dead (true positive TP) and the live cells classified as live (true negative TN) divided by the total number of classified samples. However, in the

context of highly imbalanced data set the machine learning literature suggest to use Balanced Accuracy (BA) instead.

$$Accuracy = \frac{TP + TN}{All}, \quad Balanced\ Accuracy = \frac{1}{2} \left(\frac{TP}{P} + \frac{TN}{N} \right),$$

Equation 3 - Formule of the different accuracy and balanced accuracy.

To better understand the meaning of F1 score value is necessary define previously two other measurements: *precision* and *recall*, also called positive predictive value and sensitivity, respectively. Precision tell us the percentage of our samples labeled as “positive” correctly, relative to all the samples that were labeled as “positive”. Numerically, it is the value of true positive relative to the sum of true positives plus false positive. On the other hand, recall tell us the percentage of the positive samples that were correctly labeled. Positive predictive value and sensitivity are informative numbers, it means both values were be 1.0 when we caught every positive event correctly. Both values are combined into F1 score (Figure 18), configuring a special type of average called harmonic mean that allow us to get both precision and recall into a single number combined. If one number is small between recall and precision, the F1 score is closer to the smaller number giving an appropriate score. Finally, if both measurements approach to 1, F1 score is also be close to 1.

$$F1 - score = \frac{2TP}{2TP+FP+FN}$$

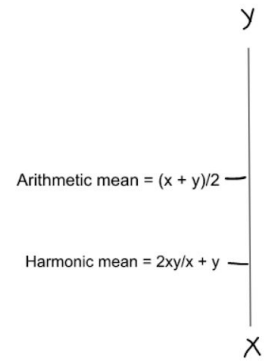


Figure 18 - Left, F1 formula and schematic, right, showing the different means. Arithmetic mean is a kind of average when x and y are equal. But when x and y are different, then it's closer to the smaller number as compared to the larger number.

We test the network performance established with the best parameters obtained with the testing data set. In order to analyze the effectiveness of our model we compute the confusion matrix which is a table with two dimensions: actual classification in columns and predicted in rows (Figure 19).

		Prediction	
		Positive	Negative
Actual Value	Dead Positive	TP	FN
	Live Negative	FP	TN

Figure 19- Confusion matrix schematic image.

Finally, to visualize the performance of the classification problem of breast cancer cells in live and dead we perform a Receiver Operating Characteristics (ROC curve).

This represents degree of separability telling how much our model is able to distinguish between the two classes. Is plotted with True Positive Rate(TPR) against False Positive Rate (FPR) defined as shown equation 4. Both values are established by the results obtained and represented on the confusion matrix (Figure 19).

$$TPR/Recall/Sensitivity = \frac{TP}{TP+FN}, Specificity = \frac{TN}{TN+FP}, FPR = 1 - Specificity = \frac{FP}{TN+FP}$$

Equation 4 - Formule of True Positive Rate(TPR) and False Positive Rate (FPR) used to plot Area Under The Curve - Receiver Operating Characteristics.

Network training and testing

The network was trained and tested in two scenarios: Untreated and treated cells. Using Pytorch framework and Python on a Graphics Processing Unit (GPU) Nvidia Titan Xp. A five hundred epochs were carried out and to find out how effective was the model different performance metrics were performed.

First Scenario: Untreated Cells

This data set was constructed with a 18099 total live cell images, and 6781 total dead cell images. We divided it into training, validation and testing set with a ratio of 80:10:10 percent (Table 9).

	Training	Validation	Testing
Live cell images	14481	1809	1809
Dead cell images	5423	679	679

Table 9 - Brightfield images with cell images without treatment, detected with Hough Circles transform and labeled as live and dead based on mean fluorescence value of PI.

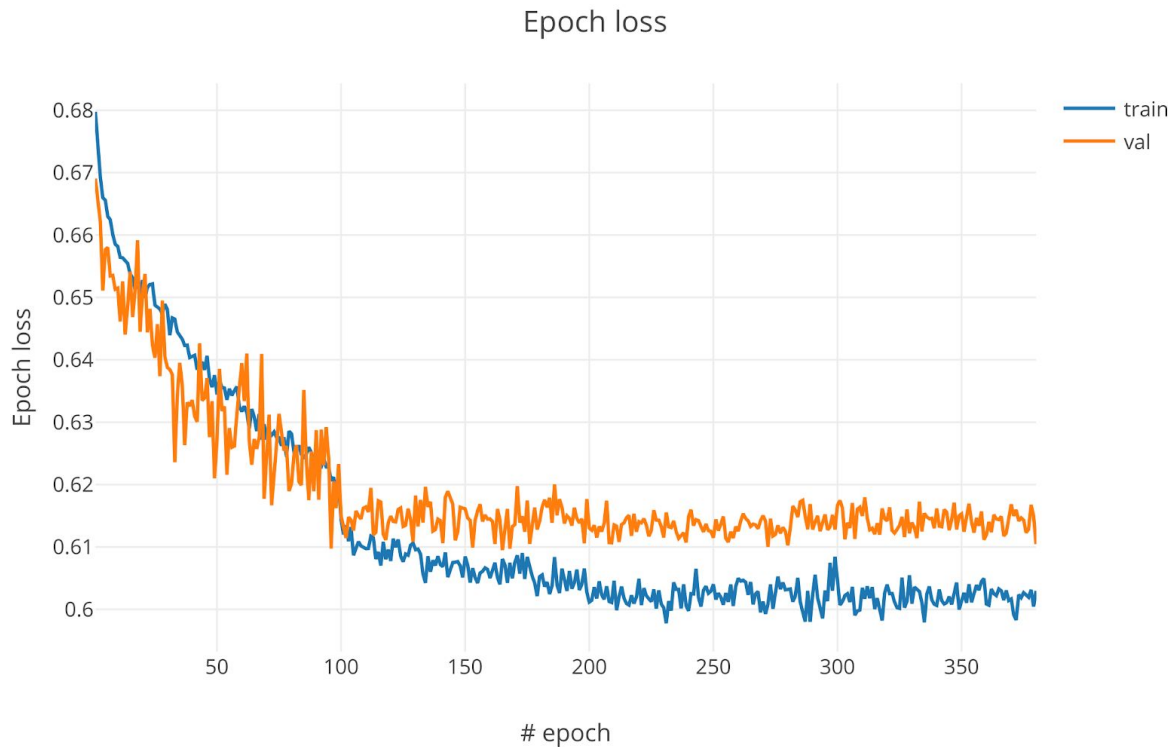


Figure 20 - Training loss function of our model with scenario 1 with two curves: training and validation. Both both continuously decrease to a value below 0.62.

We trained our network during 500 epochs. Figure 20 depicts the loss value over the whole training process for both training and validation partitions. It is observed that both losses continuously decrease up to epoch 100 where the network starts to overfit. We hypothesize this undesirable deceleration in the learning process it is due to the lack of more samples in our training data set. This represents a cut-off point where the network begins to gain greater capacity to learn about the training data set already seen but cannot generalize the validation data set by modifying the established hyperparameters. Additionally, we computed BA score on each training iteration, depicted in Figure 21. Curves show a similar behaviour when compared to the loss plot, where the generalization power of the CNN stops at iteration 100. Notice that we show a rescaled version of the BA metric different from Accuracy,

where a score of 0 means random performance of the classifier, and 1 means perfect matching between ground truth labels and the predicted ones.

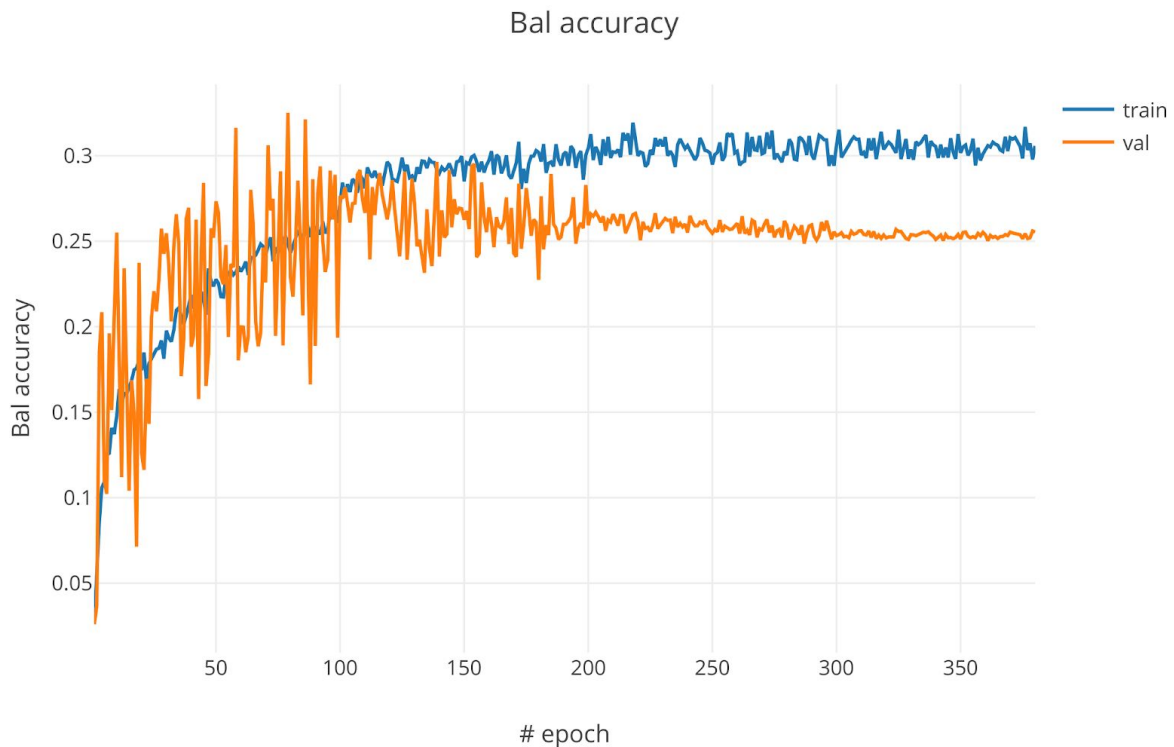


Figure 21 - Balanced Accuracy from training and validation curves from the CNN with scenario 1. After the epoch number 200 it becomes evident that there is a reduction in the ability of our model to classify unseen samples. Our best classification performance was 0.32 (adjusted BA).

Finally we plot F1-score in Figure 22. We can appreciate that the model begins to lose the capacity to discriminate positive cases around iteration 100. This is demonstrated by a top score of 0.72 after which the sensitivity and positive predictive value of our model is not comparable with the training curve anymore. A higher curve is observed for training data, which means that our model has still a greater capacity to discriminate positive cases with the already known images but insufficient data prevents it to continue improving.

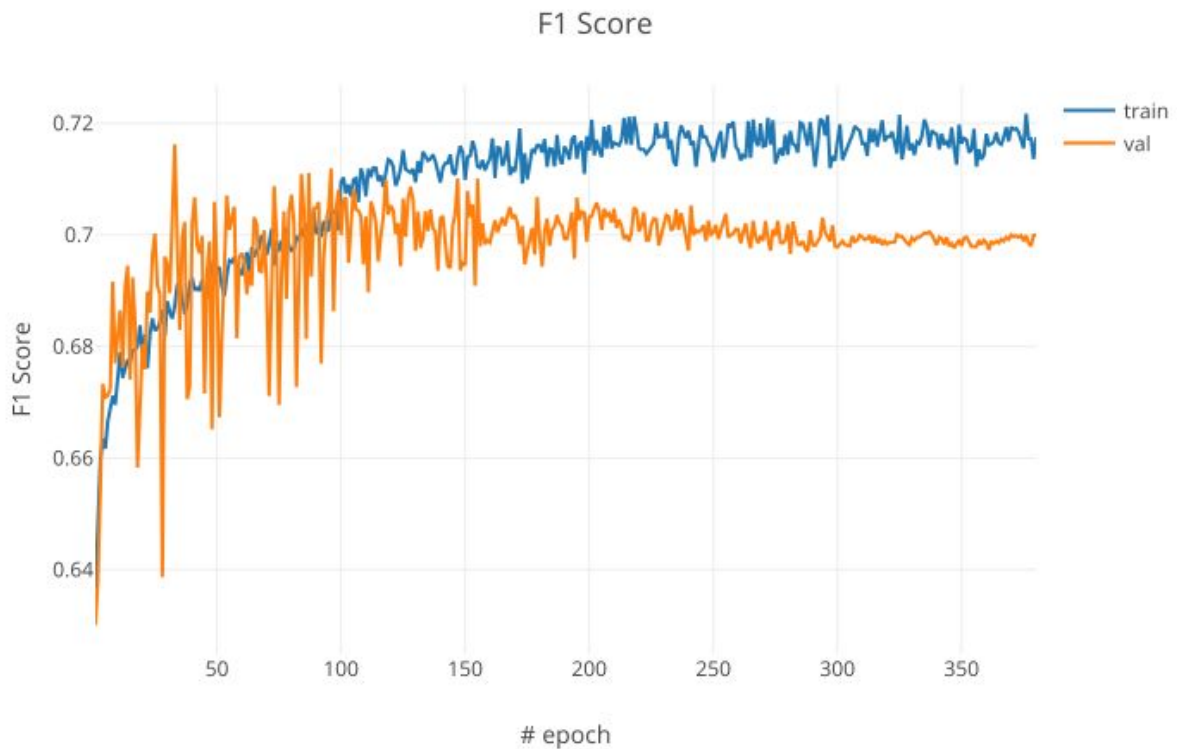


Figure 22 - F1-score of our model Training the CNN with scenario 1. Our peak value was 0.72, after the epoch number 200. Then, the model begins to lose the capacity to discriminate positive cases as reflected by the curve.

As demonstrated in all three curves, the best cut-off happens around epoch 200. Therefore, we fixed the saved network parameters at iteration 200 and use it to compute metrics over the testing set. In this way, we can obtain an unbiased evaluation of a final model over unsee cell images.

Metrics over testing set

Figure 23 shows the confusion matrix computer over all 2488 testing samples in our data set. Over a total of 679 dead cells, our model was able to correctly predict more

than half of them (378 TP). Simultaneously, when analyzing 1809 total live cells, our model was able to correctly predict 1320 input images.

		Prediction	
		Positive	Negative
Actual Value	Dead Positive	TP 378	FN 301
	Live Negative	FP 489	TN 1320

Figure 23 - Confusion matrix of our model Testing the CNN with scenario 1.

We further report the following metrics:

- *Accuracy (not balanced): 0.68*
- *Balanced accuracy (not adjusted): 0.64*
- *F1-score: 0.69*

Finally, we show the computed ROC curve in Figure 24. The curve it is augmented with a dashed line for comparison with a random performance when the model has no class separation capacity. Our model performs with an AUC of 0.695. It means there is almost 70% able to distinguish between dead and live cells. The introduction of type 1(FP) and type 2 errors (FN), like we already shown in the confusion matrix, promote the AUC less than 100%.

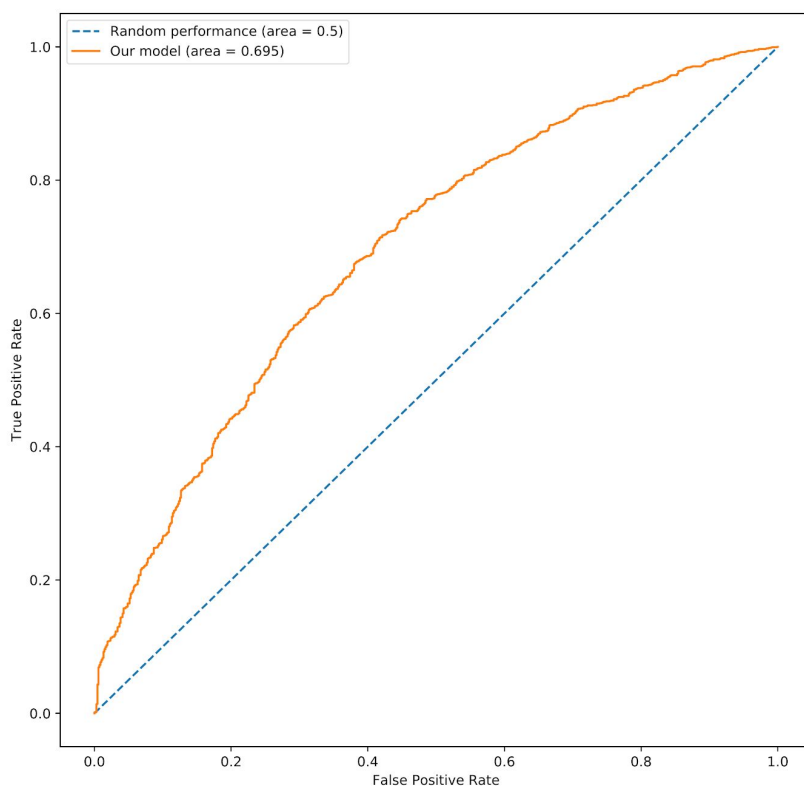


Figure 24 - AUC of 0.695 for our model over testing data from Scenario 1.

Second Scenario: Treated Cells

This data set was constructed with a 8168 total live cell images, and 3200 total dead cell images. Also divided into training, validation and testing set with a ratio of 80:10:10 percent. (Table 10).

	Training	Validation	Testing
Live cell images	6536	816	816
Dead cell images	2560	320	320

Table 10 - Brightfield images with cell images under schematic therapeutic drugs of doxorubicin and taxol., detected with Hough Circles transform and labeled in live and dead based on mean fluorescence value of PI.

We trained our network during 500 epochs. Figure 25 depicts the loss value over the whole training process for both training and validation partitions. It is observed that both losses continuously decrease up to epoch 100 where the network starts to overfit. Training curve continuously decrease to a value below 0.65 and stabilizing this above 0.64.

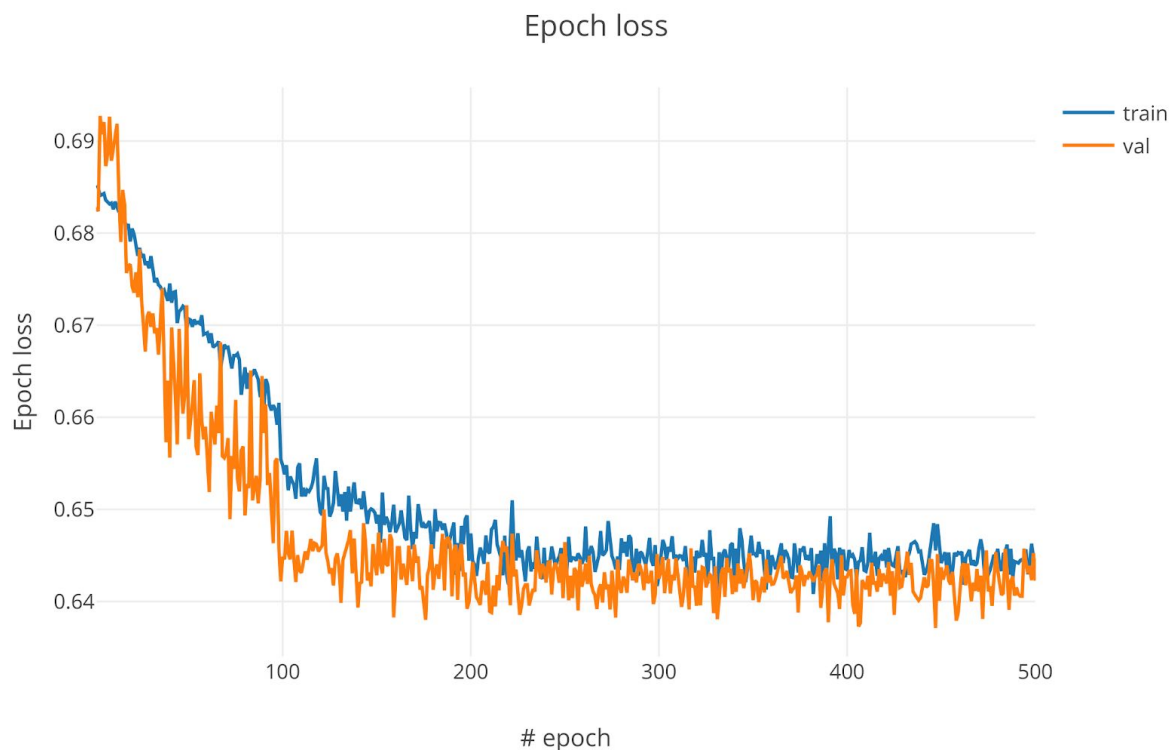


Figure 25 - Training loss function of our model with two curves: training and validation. Training curve continuously decrease to a value below 0.65 and stabilizing this above 0.64. While the validation curve accompanies the training curve but with a grated overfitting. Training with data set "celldata_doxotaxol"

While the validation curve accompanies the training curve but with a grated overfitting. This occur between the cut-off epoch range 180-200 where the model begins to stabilize the capacity to learn about the training and validation data. We hypothesize this undesirable deceleration in the learning process it is due to the lack of more samples in our training data set. This represents a cut-off point where the network begins to gain greater capacity to learn about the training data set already

seen but cannot generalize the validation data set by modifying the established hyperparameters. Additionally, we computed BA score on each training iteration, depicted in Figure 26.

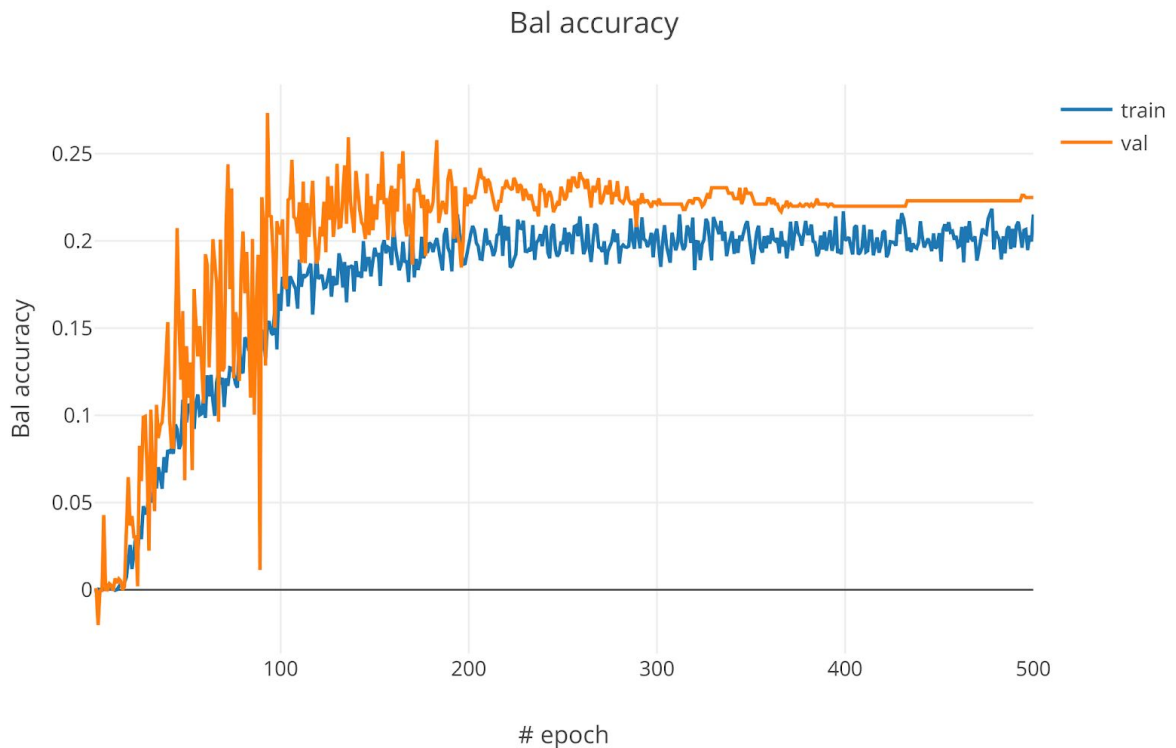


Figure 26 - Balanced accuracy of training and validation curves. The higher value it was represented by 0.27 of the balanced accuracy before to get the 2000 epoch. CNN Training with data set “celldata_doxotaxol”.

Curves show a similar behaviour when compared to the loss plot, where the generalization power of the CNN stops at iteration 100. Notice that we show a rescaled version of the BA metric different from Accuracy, where a score of 0 means random performance of the classifier, and 1 means perfect matching between ground truth labels and the predicted ones. The top score was represented by 0.27 of the balanced accuracy before to get the 200 epoch in Figure 26.

Finally we plot F1-score in Figure 27. We can appreciate that the model begins to lose the capacity to discriminate positive cases around iteration 100. This is demonstrated by a top score of 0.72 after which both curves begins to lose the capacity to discriminate positive cases. However, the validation curve show greater capacity than the training curve to discriminative positive cases.

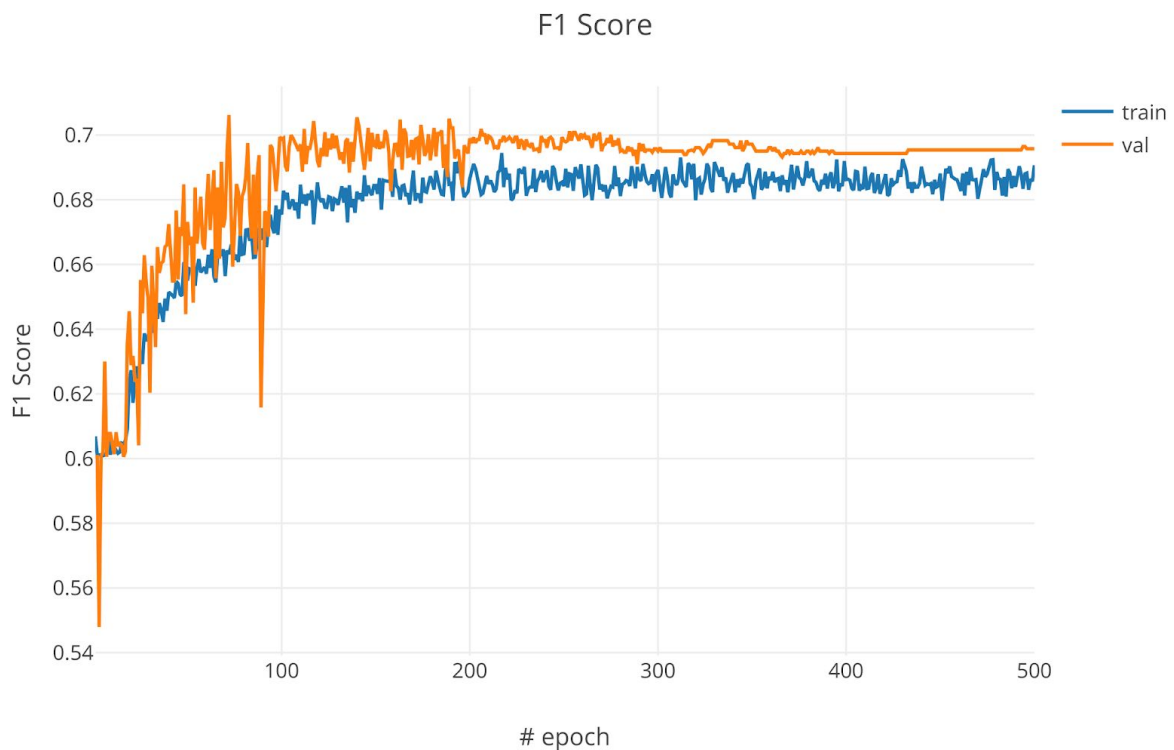


Figure 27 - F1 score of our model. The higher value was 0.70, before the epoch number 200. Then, the validation curve begins to lose the capacity to discriminate positive cases. Training with data set "celldata_doxotaxol"

As demonstrated in all three curves, the best cut-off happens around epoch range 180-200. Therefore, we fixed the saved the network parameters at iteration 190 and use it to compute metrics over the testing set. In this way, we can obtain an unbiased evaluation of a final model over unseen cell images.

Metrics over testing set

Figure 28 shows the confusion matrix computer over all 1136 testing samples in our data set. Over a total of 320 dead cells, our model was able to correctly predict more than half of them (168 TP). Simultaneously, when analyzing 816 total live cells, our model was able to correctly predict 560 input images.

		Prediction	
		Positive	Negative
Actual Value	Dead Positive	TP 168	FN 152
	Live Negative	FP 256	TN 560

Figure 28 - Confusion matrix of our model Testing the CNN with second scenario data set.

Further, we measure the following metrics:

- *Accuracy (not balanced): 0.64*
- *Balanced accuracy (not adjusted): 0.60*
- *F1-score: 0.65*

Finally, to visualize the performance of the classification problem of breast cancer cells in live and dead under drug treatment we perform an Area Under The Curve -

Receiver Operating Characteristics. The ROC curve is evidenced in figure 29. Where is plotted with a random performance to compare.

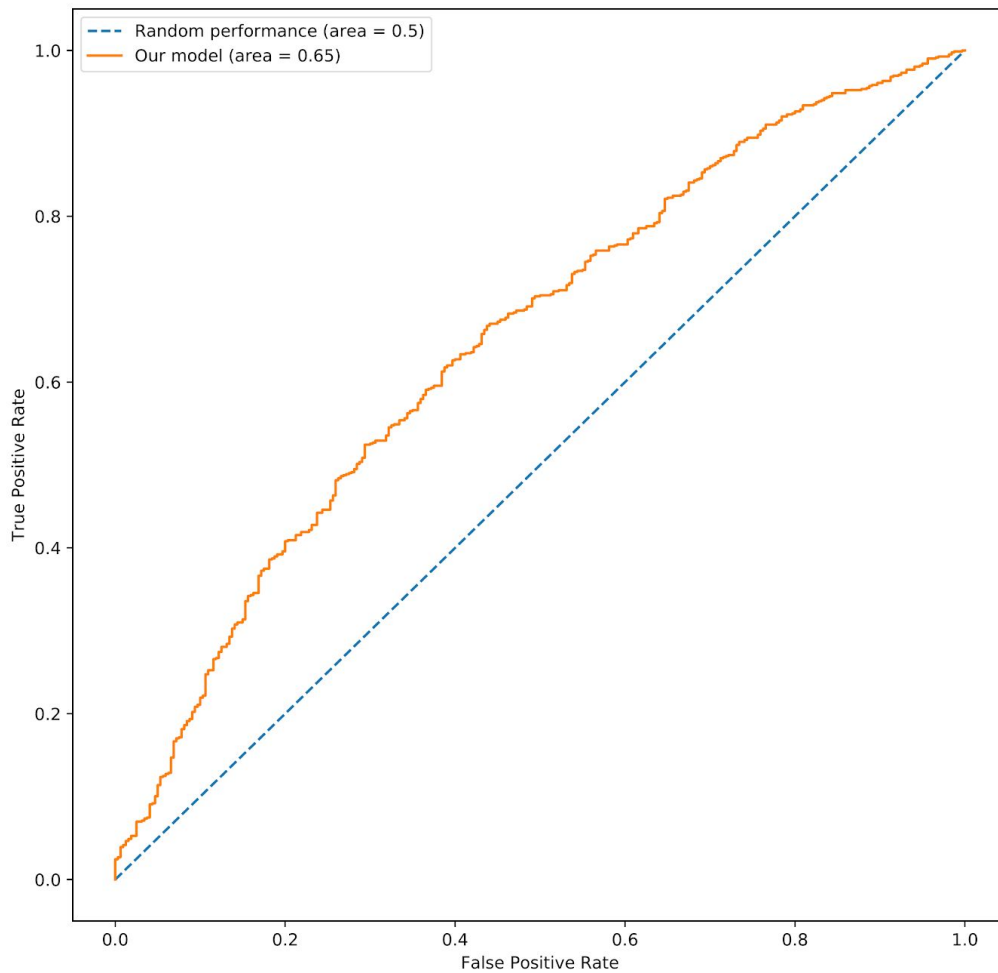


Figure 29 - AUC of 0.65 of our model Testing the CNN with “celldata_doxotaxol”.

Our model describes an AUC of 0.65. It means there is a 65% able to distinguish between dead and live cells under drug treatment with doxorubicin and taxol.

Discussion

Throughout the development of this Thesis we analyzed the morphological aspects of breast cancer cell line called JIMT-1, in particular, those related to the *in vitro* synergistic effect of chemotherapeutic agents in the treatment of breast cancer. It is uncommon to find publications that report the morphological characterization of the biological behaviour of breast cancer cells *in vitro*. The heterogeneity of the tumor biology has an important role during chemotherapeutic treatment. Even though the biological mechanism behind this heterogeneity is widely studied, the morphological responses are not. The structural differences between dead and live cancer cells may reflect the biological behaviour and serve as an extra diagnostic tool. Unfortunately many of these biological cell details cannot be precisely described, even by a trained human eye (Oei, RW., 2019). Therefore, we proposed a CNN-based classification method which provides further confirmation of the hidden features in brightfield images to detect structural differences between dead and live breast cancer cells with at least 70% of accuracy.

In this Thesis we analyzed the morphological biology of breast cancer in microfluidic model and Ibidi slide by collecting images obtained from an automatic microscope. The images collected were consolidated into a data set which has a strong potential for future biomedical image analysis research. Furthermore, to expand the morphological information, we evaluated which actual drug treatments schedule is optimal causing the higher impact over breast cancer cells.

During the image collection stage, we focused on visualizing the growth of breast cancer cells (JIMT-1). In concordance, both applied models (microfluidic and Ibidi devices) offer the possibility to visualize interactions between the cancer cells and the reaction behaviour within the microenvironment in contrast with other models of higher complexity (Sontheimer-Phelps, A. 2019).

Microfluidic models have been used to study cancer cell adhesion to endothelial monolayers as a precursor to extravasation. In these models, it was developed a cell monolayer in a microfluidic channel and interactions were studied. Our results show the importance of endothelial receptors E-selectin and CXCL12, which plays a very

important role for cancer cell adhesion (Tözeren, A. 1995; Khaldoyanidi, S. 2003; Song, J., 2009; Hsu, J.-W., 2015).

The idea of visualizing, identifying individual cell interactions within the tumour and the microenvironment, as well as the response to stimuli such as chemotherapeutics is attractive for the future development of innovative techniques. Using machine learning in cancer prediction (Kourou, K., 2015) and game theory to understand cooperation for evolution-proof therapies (Archetti, M., 2019) are already being considered on recent published work. In line with this idea, we studied the growth and development of BCC in PDMS microdevices.

In the first place, we observed the cellular concentration differences to which the BCC could be subjected within the PDMS microdevice during seeding during a period of five days. Different concentration of cells between wells and channels produce gradients difference in flow resistance (Chung, J., 2011; Barata, D., 2017) producing cellular stress or disturbing cell viability and the ability of cell division. It is known that increased pressure can affect cell division and mechanical properties of the cell, as observed in some studies (Huber, D., 2018). In this work, differences in the distribution of cells were observed, that could be affecting the growth of BCC inside of the PDMS microdevice. However, our classifying approach didn't explore this line, and focused on individual morphological cell features. Furthermore, we noticed that there were different concentrations of cells at the outlet in contrast to the inlet. In addition, these differences in the concentration of cells caused blockages in the channels after five days and poor distribution of the culture medium along the microfluidic device.

Due to the heterogeneity in BCC, it is important to keep homogeneous growth conditions. Our results show that by using this microfluidic device it was possible to track the growth of BCC. Our results show the usefulness of the system that enables the monitoring of the same cells and identification of relevant biological parameters. However, to analyse the effect of drugs over cells, it is appropriate to keep the cell culture growing under flow homogeneous conditions with Ibidi device (Song, J., 2009). Notably, cells over five days keep growing and use a live cell marker allow

better images. This favors the data set compiling tasks, getting images with excellent optical conditions for training a CNN and evaluate their performance. In order to obtain a representative data set compiling the characteristics of breast cancer cells in current therapies schedule drug treatment, the effect of DOX and PTX drugs combination schedule and LDM chemotherapy with PTX evaluation had been studied in detail.

Chemotherapeutic agents administration usually have beneficial and adverse effects. This effects depend exclusively of drug concentration. In our study we use DOX and PTX and previous clinical trials have shown benefits to combining both on breast cancer patients treatments. However, neutropenia and congestive heart failure was reported as limiting the administered dose (Holmes, F., 1999; Fisherman, J., 1996; Perez, E., 2001). Supplying a higher dose or a limitation dose does not always involve a better therapy. This situation could become affordable with diagnosis tools allowing drug treatment changes orientated to raise the level of dead cells. One possibility is to have a dead cell automatic classification done with CNNs, improving therapies while diminishing adverse effects.

LDM is a continuous chemotherapy that can be safely administered. Therefore, since these clinical trials last for long periods of time, Ibidi slides can potentially be more suitable for compiling image data sets.

Nowadays biomedical image analysis is mostly performed through open source software like FIJI. However, these tools provide very basic functionality to the user, which becomes a severe limitation for research since much of the biological analysis is performed through operations like measuring the occupied portion of the image by cells (extension). Even if FIJI supports some ML algorithms by means of plug-ins like WEKA, for segmentation we have observed that the performance is not yet accurate enough to be of practical use. Future work related with this Master Thesis should extend our results by providing a proper comparison with these broadly used tools.

Concerning the biological aspect, the effect of DOX in the first four hours reduced the percentage of area occupied by living cells and produced an increase of apoptotic cells. Those results were consistent with a raise in caspase activity. We didn't consider these aspects, by our data set could be augmented with images from this kind of treatment in order to have dead cells in a non monolayer extension. Past reports have additionally demonstrated that the schedule in which cancer cells are exposed to the chemotherapy can significantly impact the induction of proapoptotic pathways with DOX (Lee, M., 2012). PTX effect combined with DOX is widely reported as a deep synergistic inhibitory effect on the growth of different breast cancer cell lines (Wang, L. 2007, 2008). Extending our dataset with images taking into account these pharmacological aspects is important because they inhibit growth and aummentate cell death. PTX demonstrated to be and effective therapeutic agent with LDM schedule of five days, producing a higher percentage of AP cells and considerable decrease in the number of live cells. LDM therapy was widely reported in the last few years by clinical trials and in vitro studies with PTX at very low concentrations (Lien, K., 2013; Souto, M., 2015; Jiang, H., 2010). PTX in LDM (figure 9B) induced AP and inhibited the growing cells, studies suggest that it induces mitotic arrest by disrupting microtubules dynamics and activating the Spindle assembly checkpoint (Musacchio, A., 2007). Due to the disruption of microtubules, the morphology of the cell changes and became circular. Therefore, cells under taxol treatment become very similar in terms of their morphology, probably difficulting automatic classification with deep learning from brightfield images. It is in our interest to further investigate this line of research.

In summary, we succeeded in compiling a dataset that characterize the growth of BBC and drugs treatments, being the combination of PTX with LDM the best treatment to induce apoptosis and cell death.

In the field of biomedical image analysis, a CNN was implemented with success in breast cancer histology image analysis (Rakhlin A., 2018) and actin-labeled fluorescence microscopy images of three different breast cancer cells (Oei, RW., 2019). Rakhlin A. et al utilized different deep convolutional neural networks for feature extraction, including pre-trained ResNet-50, InceptionV3 and VGG-16

networks, and Light GBM. The data set is composed by a total of 400 hematoxylin and eosin stained breast histology microscopy images of four balanced classes: normal, benign, in situ carcinoma and invasive carcinoma. Their model reached an average accuracy of $87.2 \pm 2.6\%$ in 4-class classification and $93.8 \pm 2.3\%$ in 2-class non-cancer (normal and benign) vs. cancer (in situ and invasive) classification. Oei, R., et al evaluate a large number of actin-labeled fluorescence microscopy images of one human normal breast epithelial cell line and two types of human breast cancer cell line with different levels of aggressiveness. Oei et al use a VGG-16 architecture network and show an outstanding performance in cell classification tasks, even compared to a human expert (97.6% vs 78.6%). In comparison, our problem is somehow harder than its predecessors. First of all, in the case of breast cancer, histology images are fixed tissue stained with hematoxylin and eosin. This makes images in these data sets more regular, and much of the variability among images comes from the pathological characteristics to be classified. Furthermore, the actin filaments are composed of identical actin proteins arranged in long spiral chains. Consequently, convolutional neural networks learning from these images have specific visual cues to learn from in order to output accurate predictions. In comparison, our images present high shape and intensity variability, and have more subtle features that are harder to discriminate, even for the trained eye.

Relevant in our context is the work of Christiansen, E., on predicting dead state given PI fluorescence and labeled nuclei with DAPI/Höchst. They created a data set with a set of z-stacks of transmitted-light images. They reached a peak performance (recall 98%) when combining nuclear morphology information and PI. Only based on PI does not show high accurate performance because classification only based on this fluorescence images is a very challenging problem. Mainly because fluorescence is not a specific marker, which means that it only emits fluorescence with different intensities once the membrane has been compromised. This is the reason why we decide to determine a mean value fluorescence to divide the data set. Our dataset is different, we did not use z-stack and not fix the microscope in only one group of cells. Our work is orientated to predict a classification on all cell culture *in vitro* extension.

In the future, it would be interesting to extend the presented data set with extra images comprising a broader spectrum, like taxol treatment during five days. Another interesting aspect is to train different versions of our CNNs with varying the fluorescence threshold used for labeling ground truth images in our current setup. These new thresholds could be validated by a thoughtful study with human experts that can provide validation labels over a portion of the images in our data set. Additionally, avoiding unbalancing by collecting more images from new experiments would definitely improve the performance of our classifiers. Furthermore, extending the presented method to other cell lines can provide a deeper insight of the potential of CNNs to extract important visual features for cell classification.

Conclusions

In our study, we found that the autophagy process were present during the chemotherapy treatment and does not affect the final results of the treatment, which may not promote a resistance mechanism in JIMT-1. Thus, autophagy process may reflect a biological process important to reach with CNN because human eyes are not well enough in analyzing the feature. Regarding the continued application of taxol for five days observed a continuous change of morphology of the cells. Initially, they were being affected without promotion of cell death, but with continuous application came the therapeutic effect. This supports the therapeutic schemes used against resistant cancer types. This morphological changes observed may difficult the learning network process. We have proposed a CNN-based method to classify human breast-derived cell line JIMT-1 in live or dead states. A large data set of cell viability, caspase and autophagy fluorescence microscopy images was captured in order to train the network. Our results showed that CNNs can generalize from training samples to classify unseen samples. The classification features extracted by our networks are not always evident to the human eye. Further investigation on the properties of these features can provide lines for improvements leading to higher classification accuracy.

From our preliminary tests, we observed a clear difficulty when the given training data set was composed by a combination of different treatments of breast cancer. It generally lead to worse classification performance. This may indicate that some morphological features important for live/dead discrimination must be highly dependent on the specific drug or treatment.

To our knowledge, this is the first work proposing segmentation of live cell cultures that reflect biological behaviour and morphological changes of cells with and without drug treatments in order to classify cell viability. We believe our large data set of breast cancer cell line images can influence future diagnostic tools in biomedical areas.

6. References

- Amadori, D. et al. A phase I/II study of sequential doxorubicin and paclitaxel in the treatment of advanced breast cancer." *Semin Oncol.* Oct;23(5 Suppl 11):16-22 (1996).
- Arabsalmani, M. et al. "Incidence and mortality of kidney cancers, and human development index in Asia; a matter of concern." *J. Nephropathol.* 6, 30–42 (2017).
- Archetti, M. & Pienta, K. J. Cooperation among cancer cells: applying game theory to cancer. *Nat. Rev. Cancer* 19, 110–117 (2019).
- Asri H., et al. "Constructive Deep Neural Network for Breast Cancer Diagnosis." *Ifac Papers*, Volume 51, Issue 27, Pages 98-103 (2016).
- Barata, D. et al. Development of a shear stress-free microfluidic gradient generator capable of quantitatively analyzing single-cell morphology. *Biomed. Microdevices* 19, 81 (2017).
- Cheong, R., Wang, C. J. & Levchenko, A. High Content Cell Screening in a Microfluidic Device. *Mol. Amp Cell. Proteomics* 8, 433 (2009).
- Choong, H. et al. "Medical big data: promise and challenges." *Kidney Res Clin Pract.* 2017 Mar; 36(1): 3–11 (2017).
- Christiansen, E., et al. "In silico labeling: Predicting fluorescent labels in unlabeled images." *Cell.* Apr 19; 173(3): 792–803.e19 (2018).
- Chung, J., Kim, Y.-J. & Yoon, E. Highly-efficient single-cell capture in microfluidic array chips using differential hydrodynamic guiding structures. *Appl. Phys. Lett.* 98, 123701–123701 (2011).
- Fisherman, J. S. et al. Phase I/II study of 72-hour infusional paclitaxel and doxorubicin with granulocyte colony-stimulating factor in patients with metastatic breast cancer. *J. Clin. Oncol.* 14, 774–782 (1996).

Forrest, N. et al “SqueezeNet: AlexNet-level accuracy with 50x fewer parameters and <0.5MB model size” Under review as a conference paper at ICLR 2017.

Giampazolias, E. et al. “Caspase-independent cell death: An anti-cancer double whammy.” *Cell Cycle*. 17(3): 269–270 (2018).

Gozuacik, D. et al. “Autophagy as a cell death and tumor suppressor mechanism.” *Oncogene*, volume 23, pages 2891–2906 (2004).

Hanahan, D. & Weinberg, R. A. “Hallmarks of Cancer: The Next Generation.” *Cell* 144, 646– 674 (2011).

He, K.; Zhang, X.; Ren, S. Deep residual learning for image recognition. In *Proceedings of the 2016 IEEE - Conference on Computer Vision and Pattern Recognition*, Las Vegas, NV, USA, 27–30 June 2016; pp. 770–778.

HK Yuen, John Princen, John Illingworth, and Josef Kittler. Comparative study of hough transform methods for circle finding. *Image and Vision Computing*, 8(1):71–77, 1990.

Holmes, F. A. *et al.* Paclitaxel by 24-hour infusion with doxorubicin by 48-hour infusion as initial therapy for metastatic breast cancer: Phase I results*. *Ann. Oncol.* 10, 403–411 (1999).

Hsu, J.-W. *et al.* Suppression of prostate cancer cell rolling and adhesion to endothelium by 1 α ,25-dihydroxyvitamin D3. *Am. J. Pathol.* 178, 872–880 (2011).

Huang, C. *et al.* FoxM1 Induced Paclitaxel Resistance via Activation of FoxM1/PHB1/RAF-MEK-ERK Pathway and Enhancement of ABCA2 Transporter. *Mol. Ther. - Oncolytics* 14, (2019).

Huang, Z., Zhou, L., Chen, Z., Nice, E. & Huang, C. Stress Management by Autophagy: Implications for Chemoresistance. *Int. J. Cancer J. Int. Cancer* 139, (2016).

Huber, D., Oskooei, A., Casadevall i Solvas, X., deMello, A. & Kaigala, G. V. Hydrodynamics in Cell Studies. *Chem. Rev.* 118, 2042–2079 (2018).

- Jiang, H. *et al.* Low-Dose Metronomic Paclitaxel Chemotherapy Suppresses Breast Tumors and Metastases in Mice. *Cancer Invest.* 28, 74–84 (2010).
- Karuppayil, S. *et al.* “Synergistic Activation of Doxorubicin against Cancer: A Review. *Am J Clin Microbiol Antimicrob.* 1(2): 1009(2018).
- Khaldoyanidi, S. K. *et al.* MDA-MB-435 Human Breast Carcinoma Cell Homo- and Heterotypic Adhesion under Flow Conditions Is Mediated in Part by Thomsen-Friedenreich Antigen-Galectin-3 Interactions. *J. Biol. Chem.* 278, 4127–4134 (2003).
- Kourou, K., Exarchos, T. P., Exarchos, K. P., Karamouzis, M. V. & Fotiadis, D. I. Machine learning applications in cancer prognosis and prediction. *Comput. Struct. Biotechnol. J.* 13, 8–17 (2015).
- Learning-Based System to Identify Endothelial Cells Derived from Induced Pluripotent Stem Cells.” *Stem Cell Reports.* 10(6): 1687–1695 (2018).
- Leclerc, E., Sakai, Y. & Fujii, T. Cell Culture in 3-Dimensional Microfluidic Structure of PDMS (polydimethylsiloxane). *Biomed. Microdevices* 5, 109–114 (2003).
- LeCun, Yann, Yoshua Bengio, and Geoffrey Hinton. "Deep learning." *Nature* 521.7553 (2015).
- Lee, M. J. *et al.* Sequential Application of Anticancer Drugs Enhances Cell Death by Rewiring Apoptotic Signaling Networks. *Cell* 149, 780–794 (2012).
- Leist, M. & Jäättelä, M. “Four deaths and a funeral: from caspases to alternative
- Liebmann, J. E. *et al.* Cytotoxic studies of paclitaxel (Taxol) in human tumour cell lines. *Br. J. Cancer* 68, 1104–1109 (1993).
- Lien, K., Georgsdottir, S., Sivanathan, L., Chan, K. & Emmenegger, U. Low-dose metronomic chemotherapy: A systematic literature analysis. *Eur. J. Cancer* 49, 3387–3395 (Lien, K., 2013; Souto, M., 2015; Jiang, H., 2010).

Lien, K. et al. "Low-dose metronomic chemotherapy: a systematic literature analysis." *Eur J Cancer*. Nov;49(16):3387-95 (2013).

Liu, T. et al. A microfluidic device for characterizing the invasion of cancer cells in 3-D matrix. *Electrophoresis* 30, 4285–4291 (2009).

Long, H. et al. "Paclitaxel (Taxol): A Novel Anticancer Chemotherapeutic Drug." *Mayo Clinic Proceeding*. Volume 69, Issue 4, Pages 341–345 (1994).

Lowe, S. et al. "Apoptosis in cancer". *Carcinogenesis*, Volume 21, Issue 3, March, Pages 485–495 (2000).

Maetschke, S., et al. "Supervised, semi-supervised and unsupervised inference of gene regulatory networks." *Brief Bioinform*. Mar; 15(2): 195–211 (2014).

mechanisms." *Nat. Rev. Mol. Cell Biol.* 2, 589 (2001).

Musacchio, A. & Salmon, E. D. The spindle-assembly checkpoint in space and time. *Nat. Rev. Mol. Cell Biol.* 8, 379–393 (2007).

Perez, E. A. Doxorubicin and Paclitaxel in the Treatment of Advanced Breast Cancer: Efficacy and Cardiac Considerations. *Cancer Invest.* 19, 155–164 (2001).

Perou, CM. et al. "Molecular portraits of human breast tumours." *Nature*. Aug 17;406(6797):747-52 (2000).

Reichman, B. et al. "Paclitaxel and recombinant human granulocyte colony-stimulating factor as initial chemotherapy for metastatic breast cancer." *J Clin Oncol*. Oct;11(10):1943-51 (1993).

Saenz A., et al. "Targeting HER2 by combination therapies". *J Clin Oncol*. Mar; 36(8): 808–811 (2018).

Schossere, M. et al. "The Dual Role of Cellular Senescence in Developing Tumors and Their Response to Cancer Therapy." *Front Oncol.*; 7: 278 (2017).

Song, J. W. *et al.* Microfluidic Endothelium for Studying the Intravascular Adhesion of Metastatic Breast Cancer Cells. *PLOS ONE* 4, e5756 (2009).

Song, J. W. *et al.* Microfluidic endothelium for studying the intravascular adhesion of metastatic breast cancer cells. *PLoS One* 4, e5756–e5756 (2009).

Sontheimer-Phelps, A., Hassell, B. A. & Ingber, D. E. Modelling cancer in microfluidic human organs-on-chips. *Nat. Rev. Cancer* 19, 65–81 (2019).

Souto, M., Shimada, A., Barbosa, C. C., Cruz Abrahao, M. & Katz, A. Low-dose metronomic chemotherapy in metastatic breast cancer: A retrospective analysis of 40 patients. *J. Clin. Oncol.* 33, e11567–e11567 (2015).

Spitale A., et al. “Breast cancer classification according to immunohistochemical markers: clinicopathologic features and short-term survival analysis in a population-based study from the South of Switzerland.”*Annals of Oncology*, Volume 20, Issue 4, Pages 628–635 (2009).

Tanner, M. et al. “Characterization of a novel cell line established from a patient with Herceptin-resistant breast cancer.”*Mol Cancer Ther.* Dec; 3(12):1585-92 (2004).

Tözeren, A. *et al.* E-selectin-mediated dynamic interactions of breast-and colon-cancer cells with endothelial-cell monolayers. *Int. J. Cancer* 60, 426–431 (1995).

Turashvili, G. et al. “Tumor Heterogeneity in Breast Cancer.” *Front. Med.*, 08 December (2017).

Wang, L. *et al.* De-repression of the p21 promoter in prostate cancer cells by an isothiocyanate via inhibition of HDACs and c-Myc. *Int. J. Oncol.* 33, 375–80 (2008).

Wang, L. G. *et al.* Dual action on promoter demethylation and chromatin by an isothiocyanate restored GSTP1 silenced in prostate cancer. *Mol. Carcinog.* 46, 24–31 (2007).

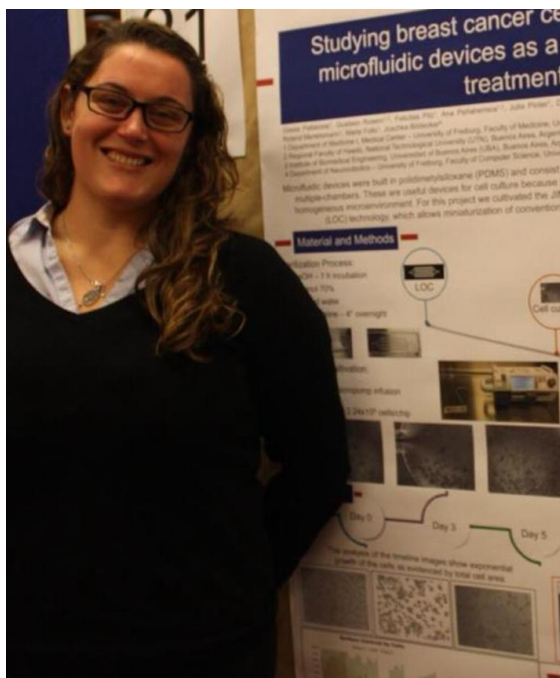
Xinzhuo, Z. and Bao Y. “A novel deep learning scheme for morphology-based classification of mycobacterial infection in unstained macrophages”. *BioRxiv*, 2019.

Xu, Z. et al. Application of a microfluidic chip-based 3D co-culture to test drug sensitivity for individualized treatment of lung cancer. *Biomaterials* 34, 4109–4117 (2013).

Zare, R. N. & Kim, S. Microfluidic Platforms for Single-Cell Analysis. *Annu. Rev. Biomed. Eng.* 12, 187–201 (2010).



About the author:



Gisela Pattarone is 32 years old. Her professional career started on her second year of Medicine. While working academically as a professor in the 3rd department of Anatomy at the University of Buenos Aires, she has improved her skills and acquired deep knowledge. She also, developed two of the most important pillars of Medicine in her opinion, the first been Teaching and the Second Research. In fact, she continues to do so today after ten years. After graduating from the School of Medicine in Buenos Aires,

Argentina in 2015, she studied English and medicine abroad in Boston, USA, in 2017. One year later, she started her Master in Biomedical Sciences at the University of Buenos Aires, Argentina and the University Albert Ludwig, Freiburg, Germany. Finally obtain my Binational: Argentina and Germany Master Degree in Science in February 2020. Currently, based in Buenos Aires, she is working and studying in Computational Neuroscience of Alzheimer's disease. She starts a highly enthusiastic and challenging PhD program.